≪리뷰논문≫ Journal of The Korean Magnetics Society, Volume 13, Number 4, August 2003

# Magnetic and Magnetostrictive Properties of Nanogranular Co-Fe Based Alloys: A Particular Emphasis on High Frequency Applications

**J. C. Sohn and D. J. Byun**

*Department of Materials Science and Engineering, Korea University, Seoul 136-701, Korea*

**S. H. Lim***

*Nano Device Research Center, Korea Institute of Science and Technology, Seoul 130-650, Korea*

A comprehensive review is given in this article on magnetic and magnetostrictive properties of nanogranular Co-Fe based alloys, with a particular emphasis on high frequency applications. Structural and physical properties are firstly described, followed by magnetic and magnetostrictive properties. Materials of both thin film and bulk forms are considered. A detailed description on high frequency characteristics of Co-Fe based soft magnetic thin films is then presented.

## I. Introduction

The development of high-frequency devices has become important from the technological point of view because of the increasing volume of information and the variety of communication media, such as mobile telephones and satellite broadcasting devices. The goal of mobile/wireless communications in the coming years will be to allow user access to the global network at any time, without regard to mobility or location. Cellular and cordless telephone communications have begun this process, but do not yet allow total communications. Continued developments in satellite communications, fiber-optic and digital microwave radio communications are aimed at this goal. Many component devices such as band-pass filters, duplexers and resonators must also conform to high-frequency bands. Surface Acoustic Wave (SAW) devices have conventionally been used for high-frequency devices [1], because they have the advantage of small size and fine filter characteristics as compared to dielectric filters and duplexers.

As a result of increasing demands by the communications industry for SAW products, many North American, European, and Japanese manufacturers of SAW devices are expanding their facilities. It is anticipated that the demand for SAW-based antenna duplexers, RF filters, and IF filters will continue to expand. As consumer adoption of mobile/wireless communications technology continues to expand, it is anticipated that RF frequencies for some systems will extend into higher GHz-band regimes. One example of this relates to the recent U.S. availability of 300 MHz of spectrum in the 5-GHz band for unlicensed radio communications. This should offer new challenges in the development of surface wave technologies and techniques at these higher frequencies that will include fabrication and power-density limitations imposed by smaller SAW device sizes. It is expected that this will include increased focus on the efficient harmonic-operational capability of SAW IDTs and reflection gratings.

Conventional SAW devices consist of a metallic thin film interdigital transducer (IDT) on top of a piezoelectric film or substrate. Application of a RF signal to the IDT generates an acoustic wave, and a similar IDT can be used to detect it. The properties and applications of these devices are well documented [2]. The use of magnetostrictive materials in SAW devices dates back to 1969, when Voltmer *et al.* introduced the surface magnetoelastic wave (SMEW) device [3]. All of the work on SMEWs used single crystal ferrite substrates, most commonly YIG ($Y_2Fe_5O_{12}$), with a thin metallic film patterned into a meander on top of the crystal [4-7]. Since the acoustic wave is wholly contained within the ferrite, these use true magnetoelastic waves. It should be noted that magnetostrictive materials have been employed in what are commonly called magnetic SAW (MSAW) devices [8], a general name for a very specific type of device. With MSAWs the acoustic wave is still generated with a piezoelectric transducer, and the magnetostrictive material serves only to modulate the acoustic velocity. With magnetically transduced SAWs (MTSAWs) the elastic wave for the most part does not reside in the magnetic material, and therefore utilizes purely acoustic rather than magnetoelastic waves. MTSAWs are therefore distinct from SMEWs and MSAWs, both in principle and in behavior.

Although the ferrites used in SMEWs have the advantage of being insulating, their magnetostriction coefficient ($\lambda$) is too low to provide device-quality insertion loss. For YIG, $\lambda$ is between 1 and 2 ppm, depending on the crystal cut [9]. Due to this and several other practical disadvantages, these devices have essentially been abandoned. MTSAWs, however, can utilize materials with far superior magnetoelastic coupling. For example, Fe-Co

*Tel: (02)958-5415, E-mail: sangho@kist.re.kr

alloys can exhibit $\lambda \approx 100$ ppm while retaining low saturation fields [10], and Tb-Fe giant-magnetostrictive materials can exhibit $\lambda$ of several hundred ppm [11, 12]. Either of these ferromagnetic alloys should ultimately provide lower insertion losses and be capable of producing commercially viable devices. However, since these alloys are conductive, a new approach to transducer design is required.

The principle advantage of MTSAWs is their use of amorphous (or polycrystalline) ferromagnetic alloys. Unlike piezoelectrics, which must be a high quality crystalline phase, they can be deposited onto any surface, and do not require high temperature processing. And piezoelectric SAW devices are expensive to produce because high quality piezoelectric crystalline substrates are costly. Moreover, SAW devices based on piezoelectric substrates cannot be readily integrated into silicon microelectronic circuits for single chip RF applications. Therefore they should be easy to integrate into RF integrated circuits. Another advantage of MTSAW is that, for the same lithographic design rule, the resonant frequency is higher than for piezoelectrics by a factor of 2, due to second-order coupling of the magnetostrictive response to the direction of magnetization. The center frequency of the SAW devices is determined by the equation $f_0 = v_p/\lambda$, where $f_0$, $v_p$ and $\lambda$ are the center frequency, the acoustic phase velocity of the SAW materials and the geometric spacing of the IDT fingers, respectively [13]. In general, choosing materials of high $v_p$ and designing IDTs of low $\lambda$ give a high $f_0$ to SAW devices. In addition, higher signal frequency applications require higher levels of anisotropy. SAW devices exhibit two types of magnetic anisotropy: an intrinsic anisotropy of the magnetostrictive material and a shape anisotropy due to the geometry of the magnetic layers in the device. These combine to form the total anisotropy of the device. A certain amount of anisotropy is needed to place the ferromagnetic resonance frequency above the devices operating frequency. This can be achieved through shape or intrinsic anisotropy or both. While a certain level of total anisotropy is needed to achieve the device operating frequency, the higher the total anisotropy, the larger the device must be. Accordingly, there is a need for SAW devices to have the lowest anisotropy consistent with the frequency of operation.

From a material point of view, it is necessary for high frequency magnetic materials to have a high ferromagnetic resonance frequency ($f_R$), a high permeability ($\mu_r$) and a high electrical resistivity ($\rho$). The high $f_R$ results from a large saturation magnetization ($4\pi M_s$) and an appropriate anisotropy field ($H_K$) according to the equation of single domain magnetic thin film along hard axis as $f_R = (\gamma/2\pi)(4\pi M_S H_K)^{1/2}$, where $\gamma$ is the gyromagnetic ratio [14]. The high $\rho$ reduces eddy current loss, which is particularly remarkable in the high frequency region. Ferrites show low $\mu_r$ and a relatively low $f_R$ due to their small $4\pi M_s$; thus, they are not suitable for high-frequency applications. Ferromagnetic metals that exhibit large eddy current losses resulting from the low $\rho$ are also not suitable for practical use in the high frequency region. Consequently, materials suitable for high-frequency application should have not only a large $4\pi M_s$ and an appropriate $H_K$, thereby increasing the $f_R$, but also a large $\rho$ thereby reducing eddy current loss [15-17]. Therefore, new magnetic materials have been developed for high frequency applications. Consequently, the applications of ferromagnetic materials for high frequency application, especially for the GHz region application, have been quite restricted [18].

Recently, nanogranular magnetic thin films have been studied to overcome the above difficult requirements of high frequency applications. The nanogranular thin films consist of nanometer scale ferromagnetic grains covered by an amorphous insulation phase. The nanogranular structure effectively suppresses the magnetocrystalline anisotropy of individual grains [19]. In addition, the increased surface area of the grains increases the exchange interaction effect. The exchange interaction effect overcomes the magnetocrystalline anisotropy, and spontaneous rotation magnetization is realized. Consequently, soft magnetism is introduced into the film. Moreover, the film itself can give a high $\rho$ as compared with metallic ferromagnetic materials, due to the insulation phase covering the metal grains. Thus nanogranular magnetic thin films have higher $\mu_r$ and lower losses even in the high frequency region.

Previous works on Fe-based nanogranular alloy magnetic thin films have shown relatively high $4\pi M_s$ values and larger magnetostriction, but with smaller $H_K$. The properties are insufficient for high frequency operation, because the resulting $f_R$ is not high enough for GHz-order high frequency applications [20-22]. On the other hand, Co-based magnetic thin films have a tendency to show a smaller $\mu_r$ caused by small $4\pi M_s$ and large perpendicular magnetic anisotropy when compared with Fe-based magnetic thin films [23, 24]. Through a combination of material properties, the possibility may exist to obtain thin films for GHz-order applications using Co-Fe-based nanogranular alloys within insulating material systems. Co-Fe-Al-O thin films with (Fe,Co) nanograins in an amorphous Al-O matrix were reported to show very good soft magnetic properties even in the GHz range [25]. The thin films also exhibit a small coercivity, mainly due to a very small (Fe,Co) grain size. Possible applications of these thin films considered so far have been inductors and noise absorbers in the GHz range. In these applications, a large magnetostriction is harmful in general and, accordingly, an alloy with a small magnetostriction was sought, mainly by adjusting the Fe/Co ratio. An Fe-Co alloy with an approximately equiatomic composition exhibits a very large magnetostriction (of the order of 100 ppm), so this alloy can be suitable for magnetoelastic device applications in the GHz frequency range.

The objective of the article presented here was to clarify, in

a controlled and detailed manner, the materials and design factors underlying the optimization of the next-generation SAW devices, the so-called "magnetically transduced SAW (MTSAW) devices". Firstly described are the results of fabricating a variety of Co-Fe-Al-O granular films, expected to have large $H_K$ and $\rho$ and to be magnetically soft, and emphasized is the relationship between the structure and magnetic properties, in particular, a high frequency response of permeability. Secondly, the magnetostrictive characteristics of nanogranular Co-Fe-Al-O thin films and the annealing effect on the properties of the films are investigated. Finally, the anisotropy field is discussed as one that can be artificially controlled among other factors to increase the ferromagnetic resonance frequency. The artificially controlled anisotropy is achieved by introducing shape anisotropy.

The scientific framework and background in preparation for the presentation of the experimental results and discussion of the work comprising are provided in this article. Three main sections are presented: the first and second sections discuss the magnetic and magnetostrictive properties of Co-Fe-based soft magnetic alloys both in bulks and in thin films including the high frequency characteristic of permeability for the films, while the third section describes the calculated effective permeability spectra and artificially controlled shape anisotropy.

Structure and physical properties of Co-Fe alloys will be described first, followed by the magnetic and magnetostrictive properties of the alloys. And then a brief summary of underlying theory that describes the ferromagnetic resonance and the calculations for the frequency dependence of permeability by computer simulation will be shown.

## II. Structure and Physical Properties of Co-Fe Alloys

### 2.1. Bulk

Co-Fe alloys near the equiatomic composition are technologically important because of their high saturation magnetization, low magnetocrystalline anisotropy and associated high permeability. The Co-Fe phase diagram is shown in Fig. 1. Co and Fe form a complete series of disordered fcc solid solutions ($\gamma$) at elevated temperatures. At low temperatures, the bcc solid solution ($\alpha$) exists up to ~75% Co.

The $\alpha$-bcc solid solutions near equiatomic composition undergo below 730°C an atomic ordering to the CsCl structure-type ($\alpha'$) and this order-disorder transformation plays an important role in determining the magnetic and mechanical properties of these materials. No order-disorder transformations are observed in alloys containing less than 30% or more than 70% Co, or in any of the alloys when cooled rapidly from 800°C or above.

In disorderd (random) solid solutions the constituent atoms, A and B, occupy the available lattice sites at random. In many alloys this disordered state is stable only at relatively high temperatures; below a certain critical temperature, long-range ordering sets in; A atoms then occupy a particular set of lattice sites and B atoms occupy another set. In the disordered state, like atoms are often adjacent to each other (AA or BB pairs), whereas ordering commonly makes all nearest neighbors unlike (AB pairs). Because the nature of the nearest neighbors in a particular alloy can influence its electronic nature, ordering usually changes the magnetic properties, sometimes dramatically. In Co-Fe alloys, at and near the composition of CoFe, ordering takes place below a critical temperature of about 730 °C, as shown in Fig. 1. In the disordered $\alpha$ phase the atoms are arranged at random on the corners and at the center of a cubic unit cell. The ordered $\alpha'$ phase has the CsCl structure, in which Fe atoms occupy only corner sites and Co atoms only the cube-center sites. Ordering produces a

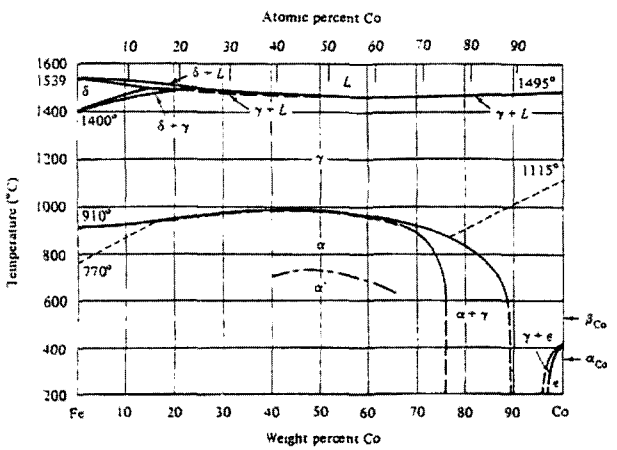


**Fig. 1.** Fe-Co phase diagram [36].

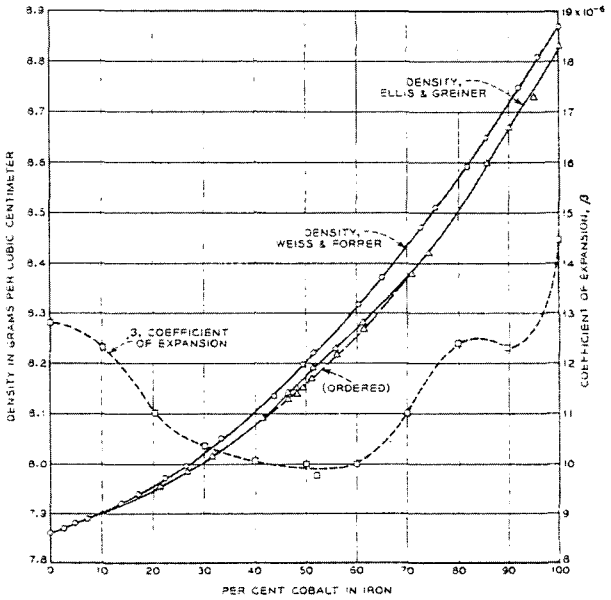


**Fig. 2.** Densities and coefficients of expansion of Co-Fe alloys [56].

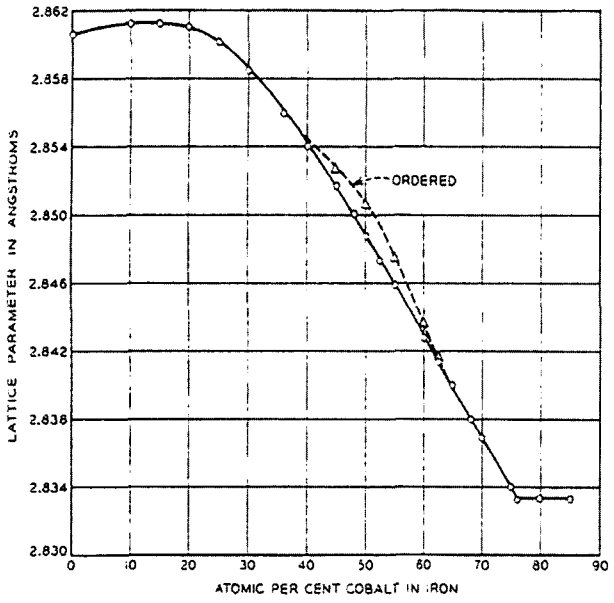


**Fig. 3.** Lattice constants of Co-Fe alloys [56].

slight increase in the saturation magnetization.

At 900 °C Fe transforms into the fcc phase $\gamma$, and at 1400 °C into the $\delta$ phase, which has the same structure as the $\alpha$ phase. At about 400 °C Co transforms, on heating, from the ε phase (hcp structure) into the $\gamma$ phase (fcc structure).

In between the areas corresponding to the single phases $\alpha$, $\gamma$, $\delta$, and $\varepsilon$ there are two-phase regions in which two crystal structures co-exist, some of the crystal grains having one structure and others the other. The dotted lines indicate the Curie point, at which the alloys become non-magnetic.

The densities of the alloys are plotted in Fig. 2. The lattice spacings of alloys containing up to 85% Co are given in Fig. 3, and show a definite expansion of the lattice on ordering, whereas most alloys show a change in the opposite direction. Coefficients of expansion are shown also in Fig. 2.

### 2.2. Thin film

Nanogranular films have been produced by a variety of means, including evaporation, co-sputtering and sequential sputtering of metal and insulator. All of the films prepared in this article were prepared by sputtering an alloy target and a composite one in $O_2$ + Ar gas. Nanogranular films are formed by a preferential oxidation of metal elements such as Al, Mg, Zr, Hf, rare earth, etc during depositions and the formation of ME (metal)-O materials as an *intergranule*. Films show good soft magnetic properties, on the other hand, are mainly prepared by co-sputtering on the rotating substrate, and both composition and morphology of the films can easily be controlled by changing the rotating speed and supplying power of each target during sputtering [47]. To reveal the structure of these films clearly, high resolution TEM observation of CoFe-ME-O based films

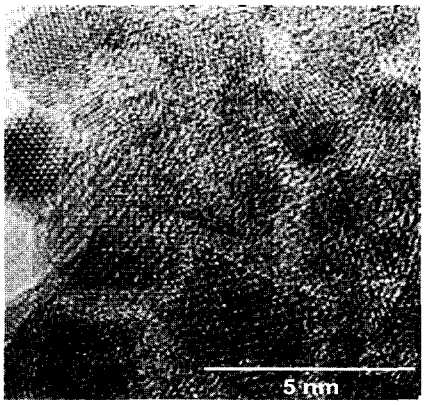


**Fig. 4.** High resolution TEM micograph for a nanogranular Co-Fe-Al-O film [47].

have been performed [48]. A micrograph of the granular structure of a Co-Fe-Al-O film is shown in Fig. 4. The granules are seen to be of relatively narrow size distribution, to be roughly spherical in shape and to be under 5 nm in diameter. The structure of granules is a bcc (Co,Fe) phase, on the other hand, that of *intergranule* is amorphous phase. The local composition of these films has been investigated by nano-focused EDX and EELS, where the spot diameter is about 2 nm. By comparing the results for the *intergranule* and granule regions, the ME concentration is low in the granule but high in the *integranule*: consequently, the concentration of Co-Fe is high in the granule, but low in the *intergranule*. Moreover, the O concentration is high in the *intergranule* and low in the granule [49].

## III. Magnetic Properties of Co-Fe Alloys

### 3.1. Bulk

Alloys of Fe and Co have the highest known values of saturation magnetization. The maximum saturation magnetization at 0 K occurs at about Fe-35% Co, although the maximum room temperature value (~24.5 kG) occurs at about 30 % Co alloy. Although Co exhibits a lower moment/atom compared to Fe, the addition of Co to Fe increases its magnetization. This is shown in Fig. 5, where the variation of the room temperature saturation moment, $\sigma_S$, with composition is given, peaking at about 30% Co. The Curie temperature, shown as dotted lines in Fig. 1, rises as Co is added to Fe up to ~15% Co, then follows (and is nearly coincident) the boundaries of the ($\alpha$ + $\gamma$) region to ~73 % Co.

The compositional dependences of induction of annealed Co-Fe alloys at various field-strengths are shown in Fig. 6. The numbers on the curves denote the field strength in Oe. Saturation at 0 K is obtained by extrapolation, and the values lie on the upper curve of Fig. 6. The second highest curve in the Fig. 6 shows $B$-$H$ at room temperature when $H$ = 17 kOe, and is substantially the $B_S$ curve. The effect of the $\gamma$, $\varepsilon$ transformation,

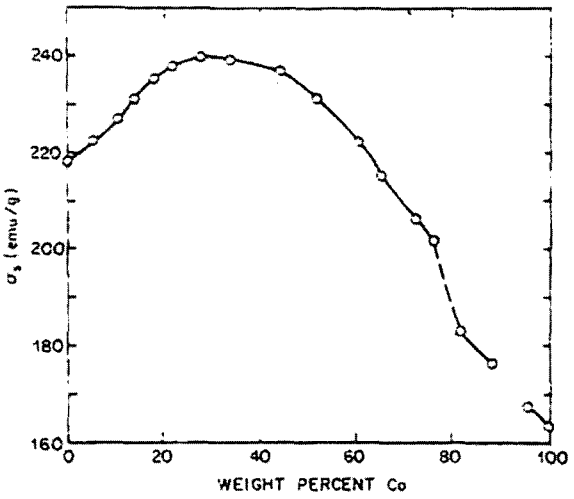


**Fig. 5.** Variation of the saturation magnetization $\sigma_S$ of Co-Fe alloys as a function of composition [60].

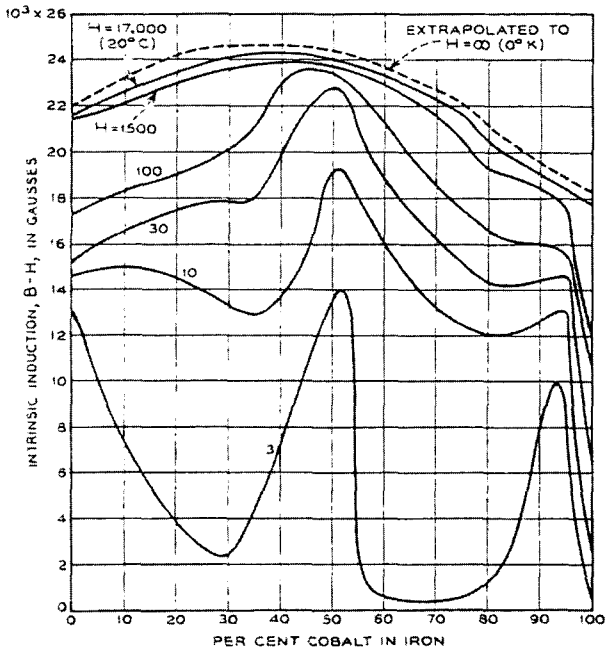


**Fig. 6.** Intrinsic induction of annealed Co-Fe alloys at various field-strengths [56].

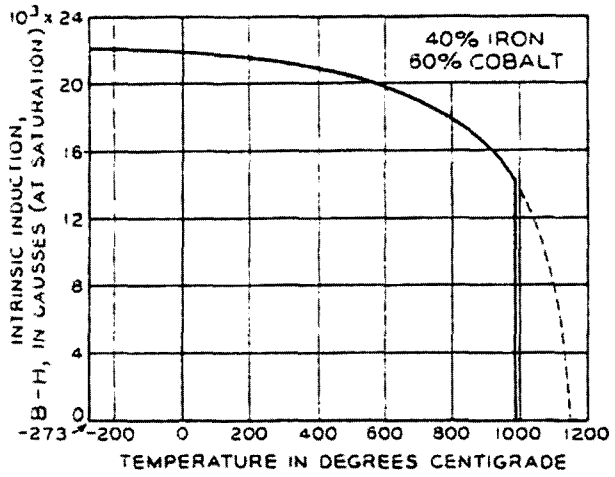


**Fig. 7.** Dependence of saturation induction $B_S$ on temperature [56].

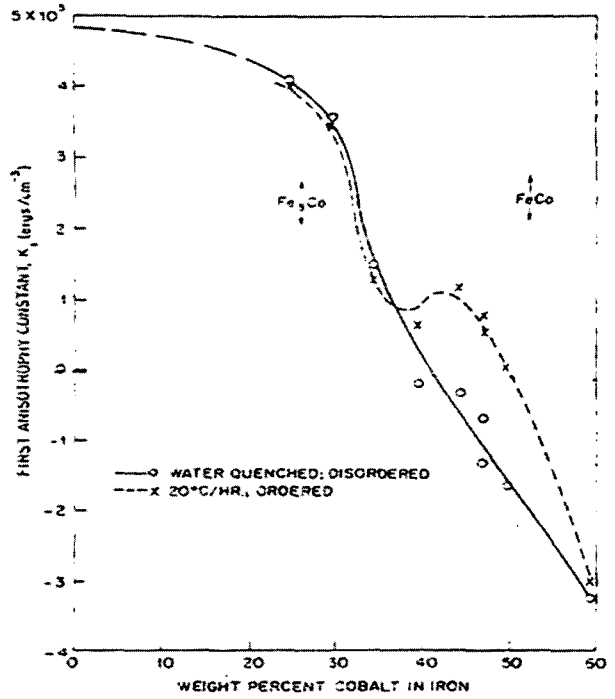


**Fig. 8.** The first anisotropy constant $K_1$ for Co-Fe alloys [60].

occurring at about 95 % Co is easily discernible in the curves for $H$ = 1500 Oe and less.

The effect of temperature on the magnetization in high fields is illustrated in Fig. 7, which shows the extrapolation to the virtual Curie point. The sharp drop in saturation at the $\alpha$, $\gamma$ transformation point, 980°C for the 60% Co alloy, is plainly visible in the curves for alloys containing 30~70 % Co.

The variation of the anisotropy constant, $K_1$, with composition is shown in Fig. 8. $K_1$ goes to zero at 40 % Co when in the disordered state, and near 50 % when in the ordered state, so it might be expected for an alloy of this composition to have a very high permeability. However, it is found that both the initial and maximum permeabilities have their maximum values at about equiatomic composition. The easy direction of magnetization changes from [100] to [111] near 41 % Co. The variation of the permeability as a function of flux density is shown in Fig. 9. The permeabilities of Co-Fe alloys show considerable variation with composition and heat treatment, as shown in Fig. 9. The rapid increase in the permeability at 45 % Co can be associated with the very low magnetocrystalline anisotropy $K_1$. The maximum permeability is increased and the coercive force reduced by heat treatment in a magnetic field. Samples annealed

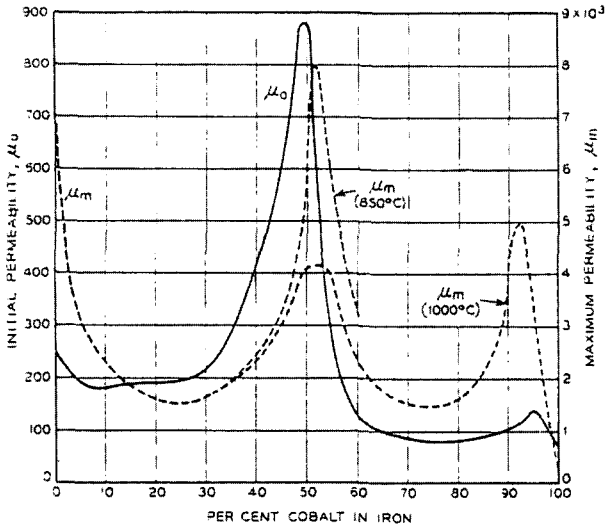


**Fig. 9.** Initial and maximum permeabilities of Co-Fe alloys. Near 50 % Co the higher $\mu_m$ is found for the lower annealing temperatures [56].

at 480 °C without a magnetic field for 15 minutes show $H_C$ = 0.70 Oe and $\mu_{max}$ = 11000, while with a magnetic field of 10 Oe, $H_C$ = 0.55 Oe and $\mu_{max}$ = 22400.

### 3.2. Thin film

*Fig. 10 shows the compositional dependence of properties* of the $(Co_{1-x}Fe_x)$AlO granular films of which Al content is 6~7 at. % and oxygen 10~13 at. %. The value of $\rho$ is around 200 μΩcm and is nearly independent of composition [Fig. 10(a)].

If the intergranular layer of Al+O is thinner, the electrical resistivity is lower. The scatter in values of $\rho$ is attributed to variations in the Al+O content. The coercivity is less than 5 Oe and is also independent of $x$ except for $x$ less than 0.2 [Fig. 10(b)]. A small $H_C$ can be explained by a random anisotropy model. A large $H_C$ in Co based films is attributed to the perpendicular magnetization originating in the appearance of hexagonal-close-packed (hcp) phase in the granules.

The compositional dependence of $B_S$ is similar to that of bulk CoFe alloys [Fig. 1(c)]. Note that $B_S$ greater than 16 kG can be obtained over a wide compositional range above $x$ = 0.3 in $(Co_{1-x}Fe_x)$ AlO films. In particular, a value of $B_S$ near 20 kG is realized near $x$ = 0.7. This suggests that $(Co_{1-x}Fe_x)$ granules in the films possess the same intrinsic magnetic properties as those in the bulk state. Particularly noteworthy is the composition dependence of $H_K$ [Fig. 10(d)]. The $H_K$ of Co-based films is near 90 Oe and decreases linearly with increase of Fe content to almost zero in Fe-based films. This variation of $H_K$ may lead to the clarification of the origin of the large $H_K$ in Co based films and will be discussed elsewhere. It is very advantageous from the practical view point that we can obtain soft magnetic granular films with any value of $H_K$ in the range from 0 to 90 Oe simply by choosing the Co/Fe ratio. Combining this result with control of the Al concentration, one can alter composition

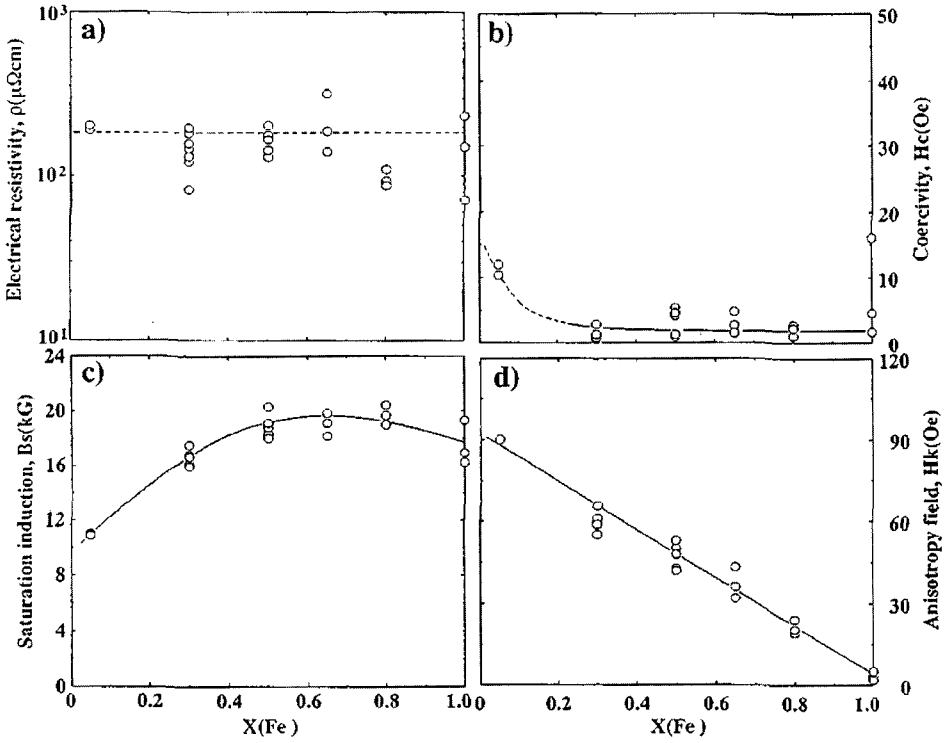


**Fig. 10.** Electrical resistivity $\rho$ (a), coercivity, $H_C$ (b), saturation induction $B_S$ (c), and anisotropy field, $H_K$ (d) as a function of Fe content in as-deposited $(Co_{1-x}Fe_x)$ AlO soft magnetic films [25].

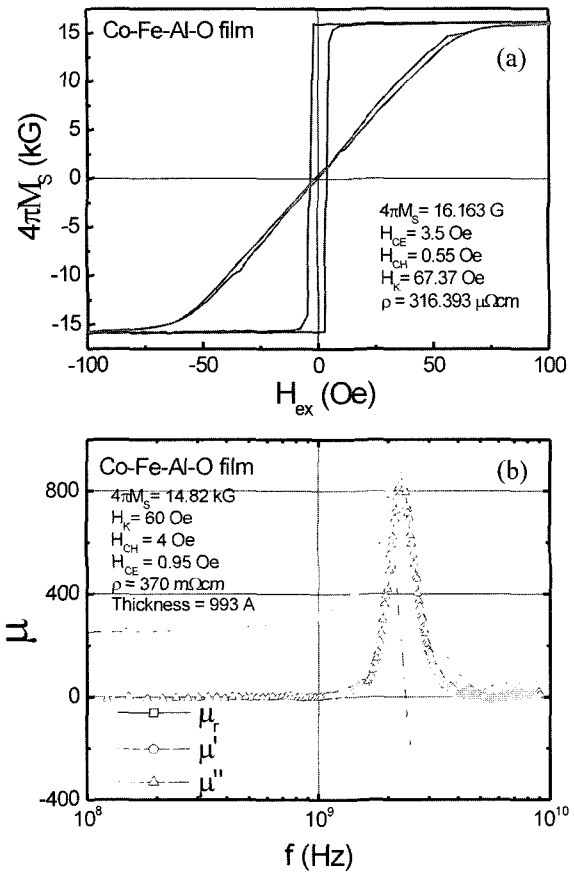


**Fig. 11.** *M-H* loops (a) and $\mu$-*f* response (b) of a Co-Fe-Al-O film.

to obtain films with optimum properties for a larger variety of magnetic devices.

Typical magnetic hysteresis loops of Co-Fe-ME-O granular films measured at RT are shown in Fig. 11(a). It is found that the granule (Co,Fe) based films have $H_C$ lower than 1 Oe for Co-Fe-Al-O films. The small value of $H_C$ is attributed to the existence of some magnetic interaction among the granules. Approaching the percolation threshold, the formation of a connecting network of small granules starts to occur. Under such conditions, the granules would prefer a magnetic closure-domain structure due to dipolar interaction, and effectively the system behaves as a multi-domain structure even though individual granules still remain single domain [50]. As a result, the magnetic properties are similar to soft magnets.

A larger $H_K$ than 60 Oe is attained, which is induced by the magnetic field during deposition. Fig. 11(b) is a typical example of the $\mu$-*f* characteristics of Co-Fe-Al-O film. The real part ($\mu'$) of permeability is nearly flat up to 1 GHz and almost consistent with the calculations based on the experimental values for $4\pi M_S$, $H_K$, $\rho$, and film thickness, and its resonance frequency exceeds 2 GHz. Although these films are the best candidates for conventional soft magnetic applications at high frequencies, another application of interest is a magnetoelastic device. For

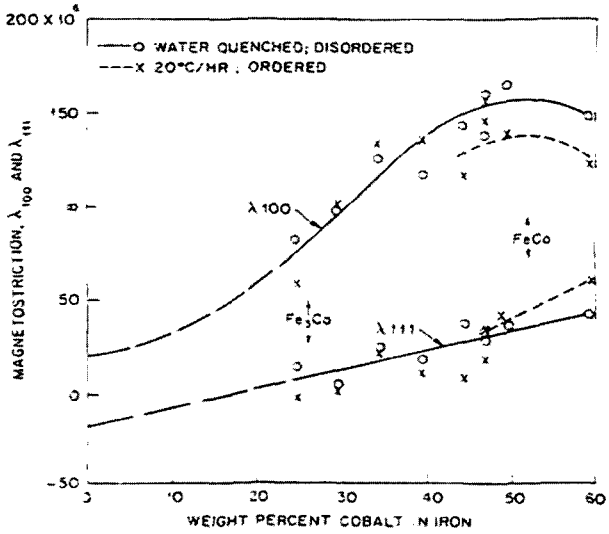


**Fig. 12.** The saturation magnetostriction in the [100] and [111] crystallographic directions for Co-Fe alloys [60].

instance, a recent high frequency SAW device requires a very good field sensitivity of magnetostriction and soft magnetic properties ($4\pi M_S \geq 10$ kG and $H_C \leq 1$ Oe). The developments on additional effects of other elements have been made to obtain a suitable film for each magnetic device application. The concentration of ME-O has a major influence on properties of Co-Fe-ME-O films, e.g., both $\rho$ and $H_K$ increase with increasing ME-O content [51]. In the case of $(Co_{1-x}\text{-}Fe_x)$-Al-O granular films [25] where Al-O content is around 30 at.%, the value of $\rho$ is around 200 μΩcm and is nearly independent of composition. $H_C$ is less than 5 Oe and is also independent of $x$ except for $x$ less than 0.1. Co-O based films are advantageous in having high $B_S$ and $\rho$; however, they show soft magnetic properties in a more limited composition range and alloy systems. Only the Ni family elements were found to improve the Co-O films, by causing them to be magnetically soft and also enhancing the $H_K$ [52]. For example, Co-Si-O films do not show soft magnetic properties, however, fairly soft magnetic properties and also a large $H_K$ than 200 Oe are observed in Co-Si-Pd-O films.

Some granular films based on the magnetic element Fe have been found to show soft magnetic properties [53-55]. However, the experimentally measured frequency dependence of their permeability is not good enough for practical applications.

An annealing in magnetic field is effective way to improve the soft magnetic properties and vary the magnitude of $H_K$ for these films. Soft magnetic properties of the film are also improved by a multi-layering with non-magnetic films like a ceramics.

## IV. Magnetostrictive Properties of Co-Fe Alloys

### 4.1. Bulk

The saturation magnetostriction ($\lambda_S$) in the [100] and [111]

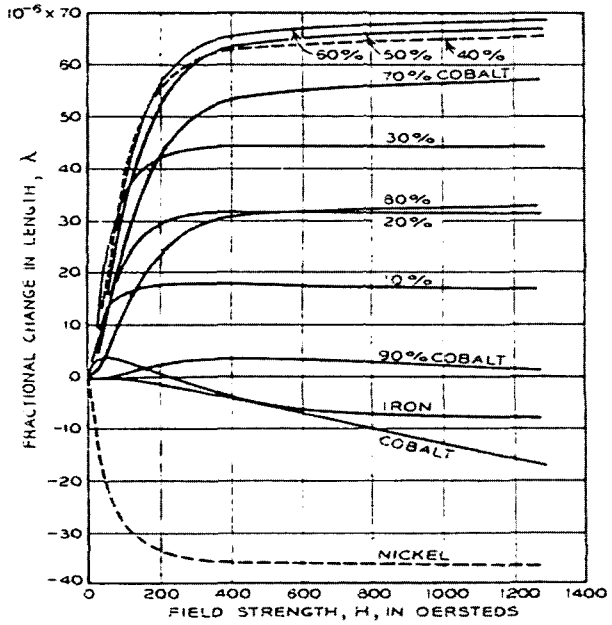


**Fig. 13.** Magnetostriction of Co-Fe alloys plotted against field strength [56].

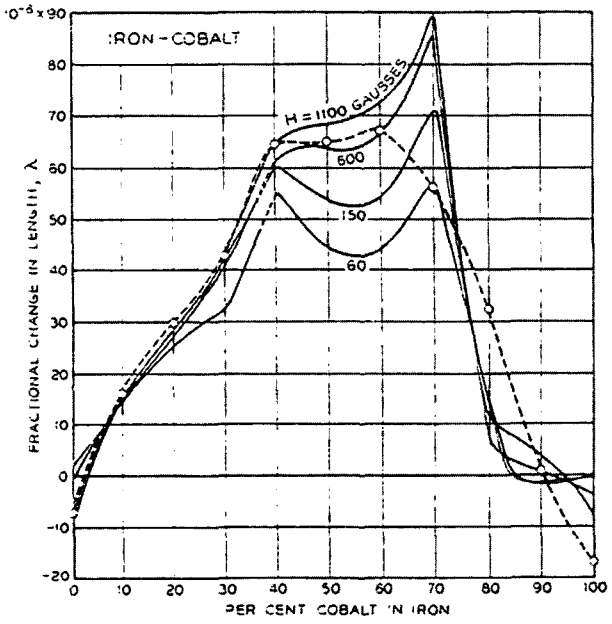


**Fig. 14.** Magnetostriction of Co-Fe alloys vs composition [56].

crystallographic directions is shown in Fig. 12 for Co-Fe alloys in the disordered and ordered states. Although the data for the ordered state are scattered, it appears that ordering lowers $\lambda_{100}$ and raises $\lambda_{111}$. Further examination of Figs. 8 and 12 shows that the ordered 50Co-50Fe alloy exhibits $\lambda_{100}$ of $150\times10^{-6}$ while $K_1 \approx 0$. For this reason, the ordered 50Co-50Fe alloy has the largest magnetostriction available in this alloy system. $\lambda$ vs $H$ for various compositions and $\lambda$ vs compositions for various field strengths of bulk polycrystalline Co-Fe alloys are shown in

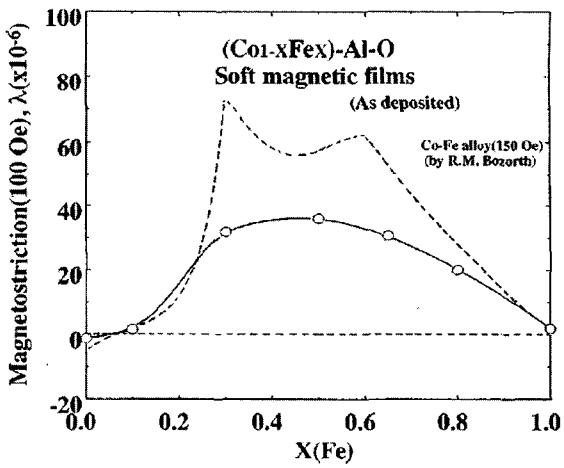


**Fig. 15.** Composition dependence of magnetostriction $\lambda$ for $(Co_{1-x}Fe_x)$-Al-O soft magnetic films [25].

Figs. 13 and 14, respectively. Taken together the results show that in moderately high fields there is an unusually large expansion of 60 to 90 ppm in alloys containing 40~70% Co.

### 4.2. Thin film

It is well known that the magnitude and field sensitivity of $\lambda$ of Co-Fe based films are important factors for magnetoelastic devices such as SAW filters. It is anticipated that the magnitude of $\lambda$ also affects the properties of high frequency magnetic devices. The magnetostriction of $(Co_{1-x}Fe_x)$-Al-O films is investigated in [25, 51]. In Fig. 15, the dotted line shows the behavior of bulk Co-Fe alloys measured in about the same magnetic field as that of the films [56]. Almost the same compositional dependence of the magnetostriction as that of bulk Co-Fe alloy is observed in the granular films, and maximum magnetostriction composition is found in $(Co_{0.5}Fe_{0.5})_{70}$-$(Al\text{-}O)_{30}$ film. This result further suggests that Co-Fe granules in the films possess the same intrinsic magnetic properties as those in the bulk state.

Any difference in magnetostriction values between bulk and granular film can be attributed to the size and crystal orientation of the grains, which are extremely fine and have a random orientation in the granular films.

Although Fe based films have proper $\lambda$ and high $B_S$ and $\rho$, the magnitude of $H_K$ is almost zero. Therefore, these films are unsuitable as for magnetoelastic devices at frequencies higher than 1 GHz, but may be chosen for lower frequency ( < 100 MHz) devices.

In the process of preparing a magnetic device, photoresist (polymer) films are coated onto the magnetic film and heated in the range 100~300 °C for hardening. Multiple coating and heating steps may be required. The magnetic film is thus subject to low-temperature annealing. It is found in [25] that $B_S$ and $\rho$ are almost independent of the annealing temperature up to 300 °C, but $H_C$ starts to decrease near 180 °C and drops to about

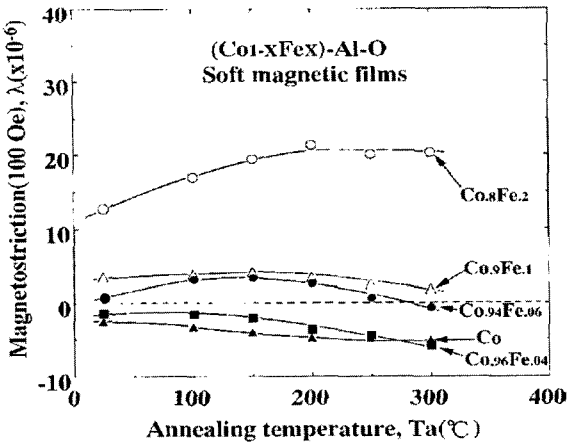


**Fig. 16.** The relationship between the magnetostriction and annealing temperature for $(Co_{1-x}$-$Fe_x)$-Al-O [25].

half its original value on annealing at 300 °C. The decrease is presumably due to structural relaxation [25]. If the anneal is carried out in a rotating magnetic field, $H_K$ begins to decrease on annealing at 140 °C and becomes almost 0 near 240 °C. The value of $H_K$, on the other hand, is constant for static field annealing up to 300 °C. These results suggest that the origin of $H_K$ of the granular soft magnetic films is a field-induced anisotropy [25]. Since the magnetostriction of soft magnetic materials varies with annealing [57], it is necessary to examine the magnetostriction in annealed Co-Fe-Al-O films to obtain optimum magnetoelastic property. Fig. 16 shows the relationship between the magnitude of magnetostriction and annealing temperature. In as-deposited films with negative values of magnetostriction $\lambda$ decreases slightly with increasing annealing temperature, but in films with positive magnetostriction a slight increase in $\lambda$ is observed. The sign of the stress in as-deposited films depends on the relative magnitude of thermal expansion in the film and substrate, and so will depend both on the film composition and on the deposition conditions. On annealing, these stresses will relax to some extent, which will affect the measured magnetostriction.

## V. High Frequency Characteristics of Co-Fe Based Soft Magnetic Thin films

### 5.1. Theory of Ferromagnetic Resonance

When a static magnetic field is applied to atoms, the total electron magnetic moment of the specimen precesses about the field direction. Assuming a high enough field to remove a domain structure, the resultant precession is considered a precessional motion of total magnetic moments. And energy is absorbed strongly from the rf transverse field when its frequency is equal to the precessional frequency. Bohr magneton of one electron in the CGS unit system is

$$\mu_B=\frac{e\eta}{2mc} \tag{1}$$

where $e$ is the electronic charge, $m$ the electronic mass, $h$ the Planck's constant, $\hbar = h/2\pi$, and $c$ the velocity of light. When a magnetic field ($H$) is applied, the exchange energy is

$$E=-g\mu_B\cdot H \tag{2}$$

$$=-g\mu_B S_z\cdot H \tag{3}$$

where $S$ is the macroscopic vector representing the total spin of the ferromagnet as quantized in the static magnetic field and $g$ is the spectroscopic splitting factor. If a magnetic field is applied in the direction of z axis, the exchange energy is equal to

$$E=-g\mu_B S_z H \tag{4}$$

Here, the allowed value for $S_z$ is ±1/2, and the energy level is split into two levels. So the energy difference between those two levels is $\Delta E = g\mu_B H$. In general, when energy is absorbed in a specific level of frequency, a condition for resonance occurrence is

$$h\nu=g\mu_B H \tag{5}$$

The relationship between angular momentum, $\overrightarrow{\mu_{orb}}$, and magnetic moment, $\overrightarrow{\mu_{orb}}$, of an electron in a circular motion is classically given by

$$\overrightarrow{\mu_{orb}}=\frac{e}{2mc}\overrightarrow{L_{orb}} \tag{6}$$

In addition, considering the spin motion of an electron, the above equation is

$$\vec{\mu}=\frac{ge}{2mc}\vec{J},$$

$$=\gamma\vec{J} \tag{7}$$

where $\gamma$ is the gyromagnetic ratio which is the ratio of the magnetic moment to the total angular momentum.

In the classical model for a precessional motion, $\vec{\mu}$ is the magnetic moment, and $\vec{J}$ is the total angular momentum. So, in this classical model, when an external field, $\vec{H}$, is applied to an isolated electron, a change of $\vec{J}$ with time is given by

$$\frac{d\vec{J}}{dt}=\vec{\mu}\times\vec{H} \tag{8}$$

In case that an external field is applied to an isolated electron, the angular frequency, $\omega$, of the precessional motion is, from Eqs. (6) and (7),

$$\omega=\frac{d\theta}{dt}$$

$$=\frac{dt}{dt}\cdot\frac{d\theta}{dJ}$$

$$=\mu H\sin\alpha\frac{1}{J\sin\alpha}$$
$$=\frac{\mu H}{J}$$
$$=\gamma H \quad (9)$$

Eq. 9 expresses the condition for resonance. Spins in ferromagnetic materials are held parallel to each other by strong exchange forces, so practically it is better to consider $\vec{M}$, the magnetic moment per unit volume of a sample, rather than $\vec{\mu}$, the magnetic moment of each spin.

$$\vec{M}=\gamma\vec{J},$$
$$\frac{d\vec{J}}{dt}=\vec{M}\times\vec{H},$$
$$\frac{d\vec{M}}{dt}=\gamma(\vec{M}\times\vec{H}) \quad (10)$$

Due to the various exchange interactions in ferromagnetic materials, $H_{eff}$, the effective applied field, should be considered for an electron in ferromagnetic materials instead of $\vec{H}$ which is for an isolated electron.

$$\vec{H}_{eff}=(\vec{H}_{app}+\vec{H}_d+\vec{H}_K+\vec{H}_{ex}) \quad (11)$$

$$\frac{dM}{dt}=\gamma\vec{M}\times\vec{H}_{app}$$
$$=\gamma\vec{M}\times(\vec{H}_{app}+\vec{H}_d+\vec{H}_K+\vec{H}_{ex}) \quad (12)$$

where $\vec{H}_d$ is the demagnetizing field, $\vec{H}_k$ the anisotropy field, $\vec{H}_{ex}\left(=\frac{2A}{M^2}\nabla^2\vec{M}\right)$ the exchange field.

### 5.2 Effects of Specimen Shape on the Resonance Frequency

When a static magnetic field ($H_z$) is applied in the direction of $z$ axis, and an ac field ($H_x$) applied in the direction of $x$ axis, the components of internal magnetic field in the specimens are equal to

$$H_x^i = H_x - N_xM_x$$
$$H_y^i - N_yM_y$$
$$H_z^i = H_z - N_zM_z \quad (13)$$

where $N_x$, $N_y$ and $N_z$ are the demagnetizing factors for magnetization along the $x$, $y$, and $z$ axes.

Substituting $H$ in eq. 10 with each component in Eq. 13,

$$\frac{dM_x}{dt}=\gamma[H_z+(N_y-N_z)M_z]M_y$$
$$\frac{dM_y}{dt}=\gamma[M_zH_x-(N_x-N_z)M_xM_z-M_xH_z]$$
$$\frac{dM_z}{dt}\cong 0 \quad (14)$$

Solutions of Eqs. 14 with time dependence $e^{jwt}$ exist. And $\chi_x$ ($M_x/H_x$) can be obtained.

$$\chi_x=\frac{\chi_0}{1-\left(\frac{\omega}{\omega_0}\right)} \quad (13)$$

$$\chi_0=\frac{M_z}{H_x+(N_x-N_z)M_z} \quad (15)$$

The angular resonance frequency is given by;

$$\omega_0=\gamma[\{H_x+(N_y-N_z)M_z\}\times\{H_z(N_x-N_z)M_z\}]^{1/2} \quad (16)$$

Consequently, the resonance conditions for specimens with different shapes are;

(a) For a flat plate with $H_z$ parallel to the plate ($N_x = N_z = 0$, $N_y = 4\pi$);

$$\omega_0=\gamma[H_z(H_z+4\pi M_z)]^{1/2}$$
$$=\gamma[H_zB_z]^{1/2} \quad (17)$$

(b) For a flat plate with $H_z$ perpendicular to the plate ($N_x = N_y = 0$, $N_z = 4\pi$);

(c) For a sphere ($N_x = N_y = N_z = 4\pi/3$);

$$\omega_0 = \gamma H_z \quad (18)$$

(d) For an infinite cylinder with $H_z$ parallel to the y axis ($N_x = N_y = 2\pi$, $N_z = 0$);

$$\frac{\omega_0}{\gamma}=H_z+2\pi M_z \quad (19)$$

Therefore, Kittles resonance condition for thin films is simply given by these equations.

$\left(\frac{\omega_0}{\gamma}\right)=H_{||}(H_{||}+4\pi M_S)$ for a field parallel to the film,

$\frac{\omega_0}{\gamma}=H_{\perp}-4\pi M_S$ for a field perpendicular to the film (20)

Practically, the first equation in eq. 20 is widely used to calculate the ferromagnetic resonance frequency for soft magnetic thin films and can be rewritten into

$$FMR=f_R \text{ or } f_0=\frac{\omega_0}{2\pi}=\frac{\gamma}{2\pi}(H_K4\pi M_S)^{1/2} \quad (21)$$

since $H_{||}(H_{||}+4\pi M_S)=H_{||}B_{||}\cong H_{||}4\pi M_S\cong H_K4\pi M_S$

### 5.3 Effects of an Angle between $H_{ex}$ and $M$ in the Film Plane on $\omega$

The equation of motion for the in-plane magnetization can be obtained by using the Smit-Beljers equation [26, 27].

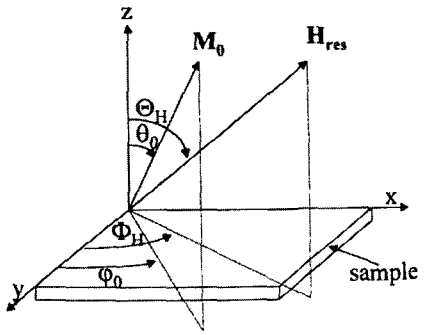


**Fig. 17.** The coordinate system, where the in-plane geometry shows the sample plane coincident with *x-y* plane [27].

$$\left(\frac{\omega}{\gamma}\right)=\{H_{res}\cos(\phi_H-\phi)+4\pi M_S+H_K\cos^2\phi\}\times\{H_{res}\cos(\phi_H-\phi)H_K\cos 2\phi\} \quad (22)$$

where $H_{res}$ is the external magnetic field for resonance to occur. In Fig. 17, the external magnetic field is applied in the in-plane direction of the specimen, that is $\Theta_H = 90^\circ$. From eq. 22, an angle dependence of resonance field ($H_{res}$) can be obtained.

$$H_{res}(\phi)=\frac{H_K}{2}[\sin^2\phi-2\cos^2\phi-2\pi M_K]+\frac{1}{2}\left\{[H_K\sin^2\phi+4\pi M_0]^2+4\left(\frac{\omega}{\gamma}\right)^2\right\}^{1/2} \quad (23)$$

For samples with anisotropic shapes, the effects of shape and demagnetization of samples on the resonance frequency should be considered. For this, Eq. 23 can be rewritten as

$$H_{res}(\phi-\delta)=H_K[\sin^2(\phi-\delta)-2\cos^2(\phi-\delta)-2\pi(M_s+P(\phi-\delta))]+\frac{1}{2}\left\{[H_K\sin^2(\phi-\delta)+4\pi(M_S+P(\phi-\delta))]^2+4\left(\frac{\omega}{\gamma}\right)^2\right\}^{1/2} \quad (24)$$

where $\delta$ is the angle deviation from $\phi$ in the resonance cavity during measurement.

The $(N_x\text{-}N_y)$ is an important factor for considering the demagnetizing effect in the in-plane direction. Here, $N_x$ and $N_y$ are the demagnetizing factors along the x and y axis, respectively.

$$N_x=K a\sin^2\varphi \quad (25)$$

$$N_y=K b\sin^2\varphi \quad (26)$$

where $a$ and $b$ are the length and width of a specimen and $K$ is a constant. The demagnetizing factors for a specimen are obtained from Eqs. 25 and 26;

$$N_x-N_y=K(a\sin^2\varphi-b\sin^2\varphi) \quad (26)$$

$$N_x+N_y=4\pi-N_z \quad (27)$$

$$N_x+N_y=K(a\sin^2\varphi-b\sin^2\varphi) \quad (28)$$

Rewritting $N_x\text{-}N_y$ using Eqs. 27 and 28,

$$N_x-N_y=(4\pi-N_z)\left(\frac{Z\sin^2\phi-\cos^2\phi}{Z\sin^2\phi+\cos^2\phi}\right) \quad (29)$$

where $Z = a / b$.

$P$ is a constant depending on a sample itself.

$$P(\phi-\delta)=P\left\{\left|\frac{Z\sin^2(\phi-\delta)-\cos^2(\phi-\delta)}{Z\sin^2(\phi-\delta)+\cos^2(\phi-\delta)}\right|\right\} \quad (30)$$

If a spin wave resonance locally occurs in a sample, a spin wave term (exchange contribution term) can be added to Eq. 22. So the equation is given by;

$$\left(\frac{\omega}{\gamma}\right)^2=\left\{H_{res}\cos(\phi_H-\phi)+4\pi M_S+H_K\cos^2\phi+Dk^2\right\}\times\{H_{res}\cos(\phi-\phi)H_K\cos 2\phi+Dk^2\} \quad (31)$$

where $D$ is the spin wave exchange constant ( $= 2A / M_S$), $A$ the exchange stiffness constant, and $k$ the spin wave vector. The spin wave vector in a localized spin wave can be expressed in the complex number as $k = i\mu$, so that $Dk^2$ is given by

$$Dk^2=-D\mu^2 \quad (32)$$

Using Eqs. 31 and 32, the following relation for resonance can be obtained;

$$D\mu^2=H_{res}-\frac{H_K}{2}[\sin^2(\phi-\delta)-2\cos^2(\phi-\delta)-2\pi(M_s+P(\phi-\delta))]-\frac{1}{2}\left\{[H_K\sin^2(\phi-\delta)+4\pi(M_S+P(\phi-\delta))]^2+4\left(\frac{\omega}{\gamma}\right)^2\right\}^{1/2} \quad (33)$$

Alternatively the resonance field with a change of an angle in the film plane is simply given by [28];

$$\left(\frac{\omega}{\gamma}\right)^2=H_{res}(H_{res}+4\pi M_S) \quad (34)$$

$$H_{res}=\frac{(H_e+H_h)}{2} \quad (35)$$

$$H_K=\frac{(H_h-H_e)}{2} \quad (36)$$

where $H_e$ *and* $H_h$ are the resonance fields along the directions of easy and hard magnetization, respectively.

### 5.4 Equation of Motion of Magnetization in the Presence of Damping

When an external magnetic field is applied to the magnetic moment, the magnetization in the absence of damping is rep-

resented by Eq. 10. In ferromagnetic materials, spin-lattice interactions occur and phenomenologically cause a magnetic loss called a damping term. There are three phenomenological damping types: Bloch-Blombergen (B-B) damping, Landu-Lifshitz (L-L) damping, and Gilbert damping.

The Bloch-Blombergen (B-B) form is given as follows;

$$\left(\frac{d\vec{M}}{dt}\right)_{x,y} = \gamma(\vec{M}\times\vec{H})_{x,y} - \frac{M_{x,y}}{T_2} \tag{37}$$

$$\left(\frac{d\vec{M}}{dt}\right)_{z} = \gamma(\vec{M}\times\vec{H})_{z} - \frac{M_z - M_0}{T_1} \tag{38}$$

where $T_1$ is identified as the spin-lattice relaxation time, $T_2$ represents loss associated with any process that disturbs or opposes the precessional motion, and $M_0$ the value of $M_z$ at stable state.

The Landu-Lifshitz (L-L) damping is in an analogy to the resistance to the motion of a top precessing in the viscose fluid, and the L-L form is given by

$$\frac{d\vec{M}}{dt} = \gamma(\vec{M}\times\vec{H}) - \lambda\left[\frac{(\vec{H}\cdot\vec{M})\vec{M}}{M^2} - \vec{H}\right] \tag{39}$$

The above equation can be rewritten as follows using the vector identical equation;

$$\frac{d\vec{M}}{dt} = \gamma(\vec{M}\times\vec{H}) - \frac{\lambda}{M^2}[\vec{M}\times(\vec{M}\times\vec{H})] \tag{40}$$

where $\lambda$ is the damping factor having the dimensions of a frequency, and the inverse of the relaxation time. It can be called the relaxation frequency, and it is the inverse of a relaxation time. The L-L damping term on the right side of Eq. 39 is a vector perpendicular to $\vec{M}$. Thus the amplitude of the precession angle can be influenced, but the magnitude of $\vec{M}$ is not affected by the damping term.

The Gilbert damping term can be obtained from Eq. 40 using the equation $\alpha\gamma/|M| = \lambda/|M|^2$ assuming that $M$ is a constant of the motion;

$$\frac{d\vec{M}}{dt} = \gamma(\vec{M}\times\vec{H}) - \frac{\alpha\lambda}{M}[\vec{M}\times(\vec{M}\times\vec{H})] \tag{41}$$

where $\alpha$ is the Gilbert damping constant. Taking the cross product of $\vec{M}$ with Eq. 41, it is found that the loss term may be modified so that Eq. 41 becomes;

$$\frac{d\vec{M}}{dt} = \gamma(\vec{M}\times\vec{H}) - \frac{\alpha}{M}\vec{M}\times\frac{d\vec{M}}{dt} + \alpha^2\gamma(\vec{M}\times\vec{H}) \tag{42}$$

where $\alpha$ is generally less than 0.05. So the last term in $\alpha^2$ Eq. 42 is sufficiently small to be neglected. Then the equation of motion including the loss term is;

$$\frac{d\vec{M}}{dt} = \gamma(\vec{M}\times\vec{H}) - \frac{\alpha}{M}\vec{M}\times\frac{d\vec{M}}{dt} \tag{43}$$

For the analysis of ferromagnetic materials, the L-L damping is generally used. In the case of small damping, both L-L and Gilbert damping terms are identical, and it can be written that $\lambda = \gamma\alpha M$. But in the case of large damping, only Gilbert damping term physically gives a reasonable result.

### 5.5 High Frequency Permeability of Soft Magnetic Thin Films

The operating frequency of magnetoelastic devices for high-speed data transmission is increasing continuously. Therefore, it is essential that the magnetic permeability of used in the devices, remains at a sufficiently high level at these higher frequencies in addition to a very good field sensitivity of magnetostriction, a high anisotropy field, a high electrical resistivity and a very low coercivity. A through understanding of mechanisms determining the frequency dependence is, therefore, essential for an optimal tuning of all the magnetic properties.

Soft-magnetic materials in high-frequency devices have a well-controlled domain pattern. In the absence of an external magnetic field, the magnetization in most of these domains is oriented perpendicularly to the flux path. In this way the high-frequency permeability is maximum because the change in magnetization is caused by a rotation of the magnetization and not by domain wall movements. Three loss mechanisms responsible for the decrease of the permeability have been known.

A. Eddy currents. Time varying magnetic fields induce eddy currents in conductors. These currents generate in turn a magnetic field that screens the external magnetic field, thereby preventing it to enter the conductor.

B. Ferromagnetic resonance. The total electron magnetic moment of the specimen precesses about the direction of the static magnetic field, and energy is absorbed strongly from the rf transverse field when its frequency is equal to the precessional frequency.

C. Dispersion of the uniaxial anisotropy. Some people mention this causes the faster decrease in permeability on increasing frequency than in calculated results on the basis of eddy currents [59, 58]. But no basic paper that really shows the effect of anisotropy dispersion on the high frequency permeability is known.

Here, we present calculated results for the frequency dependence of permeability. Two phenomena are responsible for the frequency dependence of the permeability in soft magnetic thin films: electromagnetic induction and ferromagnetic resonance. It appears that the ferromagnetic resonance mechanism is the dominating loss mechanism for highly permeable films that are thinner than 1 μm. In order to arrive at a quantitative expression for the permeability, the following assumptions are made;

(1) The film thickness $d$ is small compared to its width $w$ and length ($l$>>$d$, $w$>>$d$); consequently, the demagnetization factor equals 1 along the thickness direction and 0 along the

in-plane principal directions;

(2) The magnetic anisotropy is uniaxial and is characterized by the anisotropy constant $K_U$. The permeability is calculated in the case where an oscillating magnetic field $h(t) = h_0 exp(j\omega t)$, with a small amplitude $h_0$ and frequency $\omega/2\pi$, is applied in the plane of the film, and perpendicular to the preferential direction of the magnetization; $t$ denotes time. Under these assumptions the effect of ferromagnetic resonance and electromagnetic induction on the permeability can be quantified.

*5.5.1. Ferromagnetic Resonance*

The LandauLifshitz equation has to be solved when magnetization changes are studied in a high frequency magnetic field. This differential equation describes the change in magnetization as a function of the magnetization itself and the magnetic field. This nonlinear equation is difficult or impossible to solve for the general case. The nonlinear equation can be approximated by a linear one, using a few assumptions that are very plausible for highly permeable thin films. To solve the LandauLifshitz equation the following approximations should be made, which were also used by Amento and Rado [37] and which leads to an easily solvable linear equation: (1) the anisotropy field is small in comparison with the saturation magnetization; (2) the demagnetizing factor equals 1 in the $z$ axis, being defined as parallel with the normal of the thin film, and is equal to 0 in the $x$ and $y$ directions; (3) the damping constant is small; (4) the external field is applied perpendicularly to the anisotropy direction; (5) the applied field is small in comparison with the anisotropy field. Spenato *et al* [38] also used these approximations to study the effect of FMR in thin films. In their paper a few errors or misprints occur, which can be detected with a simple dimensional check. In this article, the results of [39] are presented. The nonlinear Landau-Lifshitz equation [40] is;

$$\frac{d\vec{M}}{dt}=\gamma(\vec{M}\times\vec{H})-\frac{\alpha\gamma}{M}[\vec{M}\times(\vec{M}\times\vec{H})] \tag{41}$$

where $\vec{H}$ is the total effective field (the sum of the applied field, the demagnetizing field and the anisotropy field), $\gamma$ is the gyromagnetic ratio, and $\alpha$ is the damping constant. $\gamma \equiv 2.1\times10^5$ m/As for Co-Fe-based alloys [41]. The values for $\alpha$ reported in literature range from 0.01 to 0.08. In the present calculations, $\alpha$ is assumed to be 0.0135. Since $\alpha$ is small, Eq. 41 can be rewritten as (neglecting terms of order higher than $\alpha^2$);

$$\frac{d\vec{M}}{dt}=\gamma(\vec{M}\times\vec{H})-\frac{\alpha}{M}\vec{M}\times\left[\frac{d\vec{M}}{dt}\times\frac{\alpha}{M}\left(\vec{M}\times\frac{d\vec{M}}{dt}\right)\right] \tag{42}$$

Assume a thin film with a demagnetizing factor of 1 in the perpendicular direction in the $z$ direction, which is defined as parallel to the normal of the film. The external magnetic field ($h_x\mathbf{e}_x$) is taken along the $x$ axis, and the magnetization of all the domains is assumed to be parallel to the $y$ direction. Furthermore, it is assumed that the change in magnetization caused by the external field is small. With these approximations $\vec{M}$ and $\vec{H}$ can be written as;

$$\vec{M}=m_x\vec{e}_x+M_S\vec{e}_y+m_z\vec{e}_z$$
$$\vec{H}=h_x\vec{e}_x+H_K\vec{e}_y+m_z\vec{e}_z \tag{44}$$

Inserting Eq. 44 into Eq. 42 and solving for $m_x$ and $m_z$ give, in the harmonic approximation, equations for $h_x$, $m_x$, and $m_z$. Defining $\mu_{xx}=m_x/h_x+1$ and $\mu_{zx}=m_z/h_x$ yields;

$$\mu_{xx}=\frac{\gamma M_S}{(\gamma H_K+i\alpha\omega)}\left[1+\frac{\omega^2(1-\alpha^2)^2}{(\gamma H_K+\gamma M_S+i\alpha\omega)(\gamma H_K+i\alpha\omega)-\omega^2(1-\alpha^2)^2}\right]+1$$
$$\mu_{zx}=\left[1+\frac{i\gamma(M_S\omega)(1-\alpha^2)}{(\gamma H_K+\gamma M_S+i\alpha\omega)(\gamma H_K+i\alpha\omega)-\omega^2(1-\alpha^2)^2}\right] \tag{45}$$

$\mu_{xx}$ is the relative permeability of interest and is equal to the parameter $\mu_r$ that is measured. The first term in the equation for $\mu_{xx}$, $\frac{\gamma M_S}{(\gamma H_K+i\alpha\omega)}$, is the most significant one. Since $\alpha$ is small, Eq. 45 can be simplified by dropping terms of order $\alpha^2$ and higher;

$$\mu_{xx}=\frac{\gamma M_S}{(\gamma H_K+i\alpha\omega)}\left[1+\frac{\omega^2}{(\gamma H_K+\gamma M_S+i\alpha\omega)(\gamma H_K+i\alpha\omega)-\omega^2}\right]+1$$
$$\mu_{zx}=\left[1+\frac{i\gamma M_S\omega}{(\gamma H_K+\gamma M_S+i\alpha\omega)(\gamma H_K+i\alpha\omega)-\omega^2}\right] \tag{46}$$

Note here, this equation is an exact solution of Gilberts form of the Landau-Lifshitz equation. Consequently, the real and imaginary parts of the relative permeability $\mu_{xx}$ due to ferromagnetic resonance effects can be obtained;

$$\mu_f'=\mu_0^2M_S^2\frac{2\mu_0K_u-\frac{\omega^2}{\gamma^2}}{\left[2\mu_0K_u-\frac{\omega^2}{\gamma^2}\right]+\left[\frac{\omega}{\gamma}\alpha\mu_0M_S\right]} \tag{47}$$

and

$$\mu_f''=\frac{\omega}{\mu}\alpha\mu_0M_S\frac{\mu_0^2M_S^2+\frac{\omega^2}{\gamma^2}}{\left[2\mu_0K_u-\frac{\omega^2}{\gamma^2}\right]+\left[\frac{\omega}{\gamma}\alpha\mu_0M_S\right]} \tag{48}$$

The effect of ferromagnetic resonance on the permeability thus depends on the material properties $K_U$ and $M_S$. The damping constant $\alpha$ cannot be derived from other material properties. $\alpha$ will be used here only as a phenomenological but generally accepted fitting parameter, as in all other FMR studies. Note that Eq. 47 reduces to the rotational permeability (Eq. 49) for small frequencies, whereas the imaginary part (Eq. 48) approaches zero.

$$\mu_{rot}=\frac{\mu_0 M_S^2}{2K_U}+1$$
$$=\frac{\mu_0 M_S}{H_K}+1$$
$$\approx\frac{\mu_0 M_S}{H_K} \text{ (in the MKS unit)}$$
$$\approx\frac{4\pi M_S}{H_K} \text{ (in the CGS unit)} \quad (49)$$

The well-known expression for the resonance angular frequency $\omega_R$ is defined as that frequency at which the real part of $\mu_{xx}$ is zero;

$$\omega_R=\gamma\sqrt{H_K M_S} \quad (50)$$

$$\text{So, } f_R=\frac{\omega_R}{2\pi}=\frac{\gamma}{2\pi}\sqrt{H_K M_S} \quad (21)$$

Because the Eq. 46 is relatively complicated, it is useful to define a figure of merit: the cutoff frequency ($f_C$), which is defined here as the frequency at which the real part of the permeability is 50 % of the initial low-frequency value [$\mu_{xx}$ ($\omega$ = 0) = $M_S$ / $H_K$]. Assuming that $\alpha$ is small and that $H_K/\alpha^2 M_S$, the relation between $H_K$ and $\omega_C$ becomes;

$$f_C=\frac{\omega_C}{2\pi}=\frac{\gamma}{2\pi}\frac{H_K}{\alpha} \quad (51)$$

5.5.2. Electromagnetic Induction

In the measurements, the effective permeability is measured, which is the intrinsic permeability reduced by eddy currents. The effect of eddy currents on the effective permeability has long been known. For completion, the derivation of the relevant relations will be given below.

Consider a plate finite in the $x$ and $y$ directions, with an intrinsic relative permeability $\mu_r$ and having a finite thickness $d$ in the $z$ direction. A harmonic magnetic field is applied in the $x$ direction: $H = H_0\exp(i\omega t)e_x$. Eddy currents will be generated in the $y$ direction. These eddy currents will screen the $H$ field inside the plate and, because the plate is infinite, will have no effect on the $H$ field outside the field. The relevant Maxwell equations to be solved are;

$$\nabla\times\vec{E}=-\mu_0\mu_i\frac{\partial\vec{H}}{\partial t}$$
$$\nabla\times\vec{H}=\vec{J}=\sigma\vec{E} \quad (52)$$

In these equations, $\vec{J}$ is the current density, $\sigma$ is the electrical conductivity, and $\mu$ is the magnetic permeability. Combination of these equations and using $\partial\vec{H}/\partial t=i\omega\vec{H}$, gives the following differential equation;

$$\frac{\partial^2 H_x(z)}{\partial z^2}=i\omega\sigma\mu_0 H_x(z) \quad (53)$$

Using the boundary conditions $H(d/2) = H(-d/2) = H_0$, the solution of this differential equation is;

$$H_x(z)=H_0\frac{e^{(1+i)z/\delta}+e^{-(1+i)z/\delta}}{e^{(1+i)d/2\delta}+e^{-(1+i)d/2\delta}}e^{i\omega t} \quad (54)$$

In this equation, $\delta$ represents the skin depth and is equal to $\sqrt{2/(\omega\sigma\mu_0\mu_i)}$. The applied oscillating magnetic field induces eddy currents which screen the magnetic field inside the film, as described by Maxwells equations. Therefore, the magnetic field only penetrates over a characteristic length $\delta$, which is the skin depth. This parameter is related to the resistivity $\rho$ and the intrinsic relative permeability $\mu_i$ of the thin film material by [41];

$$\delta=\sqrt{\frac{2\rho}{\omega\mu_0\mu_i}} \quad (55)$$

with $\mu_0 = 4\pi\times 10^{-7}$ H/m, the permeability of vacuum. Integration of Eq. 54 over $z$, multiplication by the intrinsic permeability $\mu_i$, and dividing by $H_0 e^{i\omega t}$ gives the average effective permeability due to electromagnetic induction;

$$\mu_e\equiv\mu_e'-i\mu_e''=\mu_i\frac{(1-i)}{d/\delta}\frac{e^{(1+i)d/\delta}-1}{e^{(1+i)d/\delta}+1} \quad (56)$$

$\mu''$ is defined as minus the imaginary part of the relative permeability, and $d$ is the film thickness. This equation leads to the well-known expressions for the real and (minus) the imaginary parts of $\mu_e$;

$$\mu_e'=\frac{\mu_i}{\beta}\frac{\sinh\beta+\sin\beta}{\cosh\beta+\beta+\cos\beta} \quad (57)$$

and

$$\mu_e''=\frac{\mu_i}{\beta}\frac{\sinh\beta-\sin\beta}{\cosh\beta+\beta+\cos\beta} \quad (58)$$

where $\beta$ is defined as $d/\delta$. In the application of Eqs. 57 and 58, to calculate the effect of electromagnetic induction on $\mu_e(\omega)$, the permeability $\mu_i$ can be approximately obtained by the rotational permeability $\mu_{rot}$ (Eq. 49). This approximation is valid, since the field is applied perpendicular to the preferential direction of the magnetization and therefore rotation is the dominant magnetization reversal mechanism.

Summarizing, the effect of electromagnetic induction on the permeability (Eqs. 57 and 58) is governed by the material properties $M_S$, $K_U$, and $\rho$ and the geometrical quantity $d$.

5.5.3. Combined Effect

A relation between the intrinsic permeability and the frequency has now been found. In the measurements, the effective permeability is measured, which is the intrinsic permeability reduced by eddy currents. Eqs 47 and 48 represent the intrinsic frequency-dependent permeability. Since this permeability is not position-dependent, the expression for $\mu_f'$ and $\mu_f''$ [Eqs. 47 and 48] can be inserted for $\mu_i$ into Eqs. 57 and 58. This gives an expression for the frequency-dependent permeability in which both the eddy currents and the ferromagnetic resonance are taken into account;

$$\mu_e' = \frac{1}{\beta}\left\{ \mu_0^2 M_S^2 \frac{2\mu_0 K_u - \frac{\omega^2}{\gamma^2}}{\left[2\mu_0 K_u - \frac{\omega^2}{\gamma^2}\right]^2 + \left[\frac{\omega}{\gamma}\alpha\mu_0 M_S\right]^2} + 1 \right\} \frac{\sinh\beta + \sin\beta}{\cosh\beta + \cos\beta} \quad (59)$$

and

$$\mu_e' = \frac{1}{\beta}\left\{ \frac{\omega}{\gamma}\alpha\mu_0 M_S \frac{\mu_0^2 K_S^2 + \frac{\omega^2}{\gamma^2}}{\left[2\mu_0 K_u - \frac{\omega^2}{\gamma^2}\right]^2 + \left[\frac{\omega}{\gamma}\alpha\mu_0 M_S\right]^2} + 1 \right\} \frac{\sinh\beta - \sin\beta}{\cosh\beta + \cos\beta} \quad (60)$$

In this equation, the only degree of freedom is $H_K$. $\rho$ and $M_S$ are known from other measurements. The value for $H_K$ must be taken such that the calculated low-frequency permeability is in agreement with the measured one. This value must also be in reasonable agreement with the value of $H_K$ obtained from *B-H* loop measurements. Note here that the exchange energy term is not taken into account in the derivation presented here.

### 5.6. Calculated Effective Permeability Spectra

The effects of the parameters $4\pi M_S$, $H_K$, $\alpha$, $d$ and $\rho$ on the permeability spectra are examined, using Eqs. 59 and 60, inside a frequency range by holding one of the parameters constant and changing the others.

5.6.1. Influence of the Film Thickness

An example showing the importance of thickness is given in Fig. 18, where calculated values of $\mu'$ and $\mu''$ using Eqs. 59 and 60 are plotted as a function of frequency for four different values of $d$ with $g = 2$, $\alpha = 0.05$, $4\pi M_S = 14$ kG, $H_K = 30$ Oe, and $\rho = 1000$ μΩcm. It is seen that a high permeability is maintained in high frequency range with decreasing value of $d$. The imaginary part of the complex permeability $\mu''$ shows a high resonance at small $d$ value. The film thickness is an important factor to control eddy current loss. The thinner films exhibit a high permeability maintained in higher frequency range due to the lower eddy current loss. This behavior can be attributed to eddy current effects inside the thin film. If an ac field is applied to a conducting material, circulating currents (eddy currents) are induced inside the material, having, in accordance with Lenzs law, such a direction that they create a field in opposition to the field that creates them. These currents depend on the material resistivity, permittivity, permeability, and the ac field frequency. One must note that the permeability calculated in this article is not an intrinsic value but an apparent value, due to the screening effects created by eddy currents at the surface of the sample. It is found in the figure that the proper thickness for a low loss factor over GHz ranges exists under the conditions that the high electrical resistivity and magnetic properties of the film are kept constant with the thickness. The permeability is independent of the thickness for the films with d < 2 μm. But, for $\rho < 1000$ μΩcm, it is expected that the thickness range where the permeability is independent of the thickness should be lower. In general, a good agreement between theoretical and experimental values of the cut-off frequency can be observed for sample thicknesses larger than 2 μm. For smaller thicknesses which are about the skin depth, one can obtain a cut-off frequency higher than the one measured.

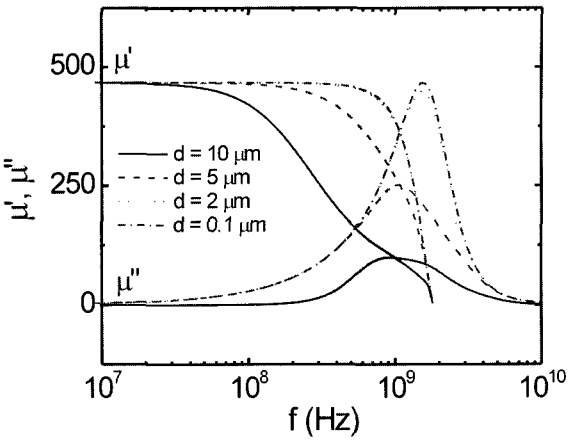


**Fig. 18.** Calculated frequency dependence of the complex permeability due to both electromagnetic induction and ferromagnetic resonance for several values of thickness.

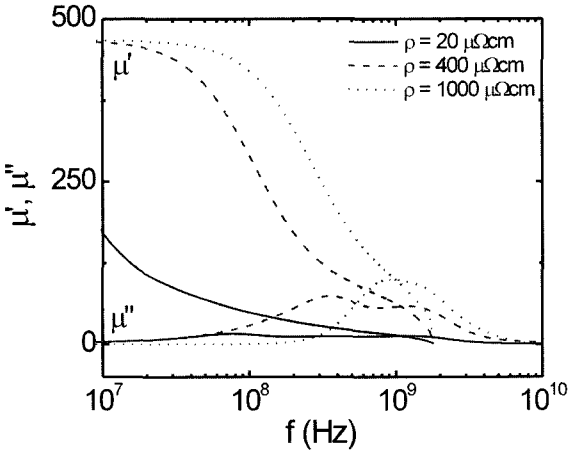


**Fig. 19.** Calculated frequency dependence of the complex permeability due to both electromagnetic induction and ferromagnetic resonance for several values of the resistivity.

5.6.2. Influence of the Electrical Resistivity

To explain the frequency-dependence of the permeability due to spin rotation of thin ferromagnetic films, a model taking into account the influence of eddy currents should be proposed such as Eqs. 59 and 60. When a conductive thin film is subjected to a high-frequency exciting field, eddy currents are induced in the film and they create screening effects at the surface of the film. The exciting field only penetrates into the film to a certain depth, the skin depth, and makes the apparent permeability roll off at high frequencies. Figs. 19 and 20 show film frequency

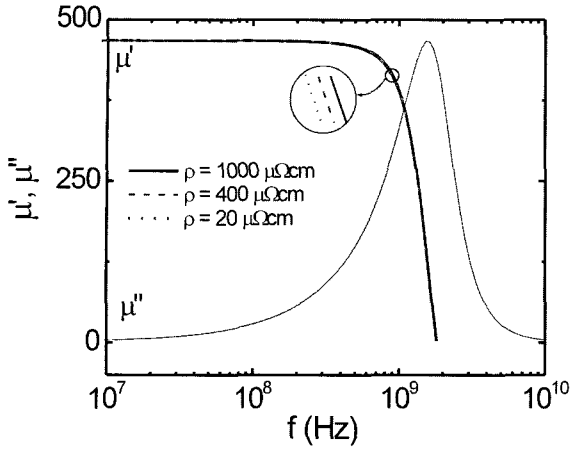


**Fig. 20.** Calculated frequency dependence of the complex permeability due to both electromagnetic induction and ferromagnetic resonance for several values of the resistivity.

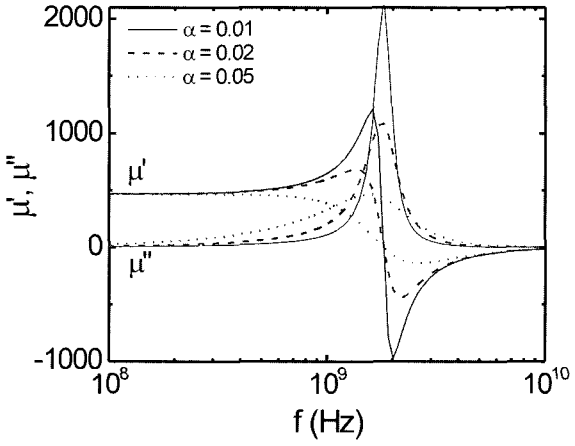


**Fig. 21.** Calculated frequency dependence of the complex permeability due to both electromagnetic induction and ferromagnetic resonance for several values of the damping constant.

dependence of calculated permeability for electrical resistivity $\rho$ = 20, 400 and 1000 μΩcm at 10 μm and 0.1 μm thick films, respectively. For the 10 μm thick film, a high permeability is maintained up to higher frequencies with increasing values of $\rho$ due to the lower eddy current loss for high resistivity films. But films with $d$ = 0.1 μm exhibit a behavior that permeability is independent of the electrical resistivity due to the small magnetic induction effect in very thin films.

5.6.3. Influence of the Damping Constant

The influence of the damping constant on the permeability is shown in Fig. 21, with $g$ = 2, $d$ = 0.1 μm, $\rho$ = 1000 μΩcm, $4\pi M_S$ = 14 kG and $H_K$ = 30 Oe. A very sharp resonance of a large magnitude is shown for low values of $\alpha$. For high values of $\alpha$ (> 0.05), the resonance curve is strongly damped. The spectrum is relaxed with the increase of damping coefficient. As $\alpha$ increases the level of $\mu'$ at low frequency stays the same but the cut-off

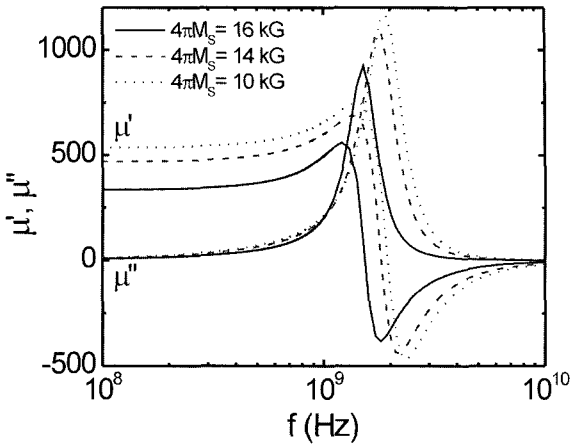


**Fig. 22.** Calculated frequency dependence of the complex permeability due to both electromagnetic induction and ferromagnetic resonance for several values of the saturation magnetization.

frequency decreases. $\mu''$ shows a wide resonance peak, and its level is low. In addition, the resonance frequency has shifted slightly downward, and the spectral magnitude at resonance is decreased by a factor of about 4. Great spectra relaxation is seen for further increases in the damping coefficient; $\mu'$ no longer goes negative, and the resonance frequency shifts to values below the GHz range. There is no unique physical interpretation of $\alpha$ since the line width of the resonance is determined by two indistinguishable effects. These are extrinsic effects such as a spread in the magnetic properties (e.g., the inhomogeneity in $K_U$ values giving rise to different resonance frequencies) and intrinsic effects, which are related to the interaction between electrons and spins (in fact the magnetization), between conduction electrons and between the lattice and such systems as the electron-spin system and the conduction electron system. There is an energy exchange between those systems and the specific relaxation times. Thus $\alpha$ will be used here only as a phenomenological but generally accepted fitting parameter, as in all other FMR studies.

5.6.4. Influence of the Saturation Magnetization

Fig. 22 shows the frequency dependence of the calculated relative permeability for three different values of $4\pi M_S$ with $g$ = 2, $\alpha$ = 0.02, $H_K$ = 30 Oe, d = 0.1 μm and $\rho$ = 100 μΩcm. As $4\pi M_S$ increases, the level of $\mu'$ at low frequency increases but the cut-off frequency is practically unchanged. The imaginary part of the complex permeability $\mu''$ shows a higr resonance peak at high value of $4\pi M_S$. The behavior of $\mu'$ agrees with the Stoner and Wolfarth theory [42], which gives for the permeability at low frequency, the value $\mu' = 4\pi M_S / H_K$.

5.6.5. Influence of the Anisotropy Field

Eqs. 59 and 60 are used to determine the permeability of the thin film with $4\pi M_S$ = 14 kG, $g$ = 2, $\alpha$ = 0.02, d = 0.1 μm, and $\rho$ = 100 μΩcm for three different values of the anisotropy field. The level of $\mu'$ at low frequency is low and the cut-off fre-

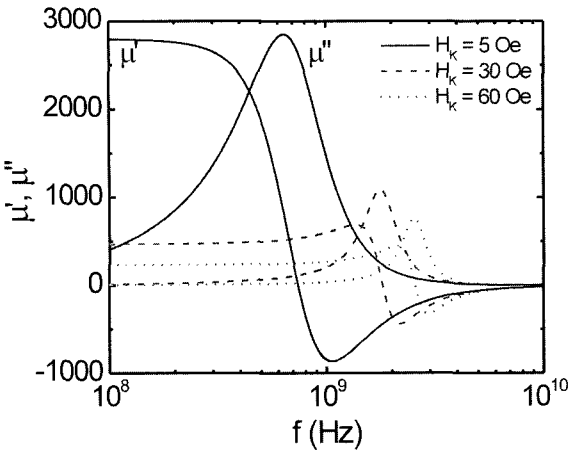


**Fig. 23.** Calculated frequency dependence of the complex permeability due to both electromagnetic induction and ferromagnetic resonance for several values of the anisotropy field.

quency is high at a high $H_K$ value (Fig. 23). $\mu''$ shows a low resonance peak at a high $H_K$. The behavior of $\mu'$, as function of $H_K$, still agrees well with the Stoner and Wolfarth theory. It is known that the permeability is controlled by magnetization mechanisms of Bloch wall displacement and spin rotation mainly. When the exciting field is applied parallel to the in-plane easy axis of the materials showing in-plane anisotropy, the magnetization reversal is mainly due to Bloch wall displacement. In this configuration the permeability becomes nearly one. When the exciting field is applied perpendicular to the easy axis, the magnetization reversal is taking place by spin rotation. This consideration leads to the conclusion that for anisotropic magnetic thin films, significant values with a low exciting field are obtained only when the applied field is perpendicular to the easy axis.

At low frequencies, when the exciting field is applied along the easy axis, the initial permeability, due to the motion of Bloch walls, is large and rolls off at about a few tens of kilohertz. When the exciting field is applied perpendicular to the easy axis, the permeability is generally low and is due to spin rotation. In this case the roll-off frequency may approach a few hundred megahertz and can even reach over a few gigahertz with a shape anisotropy introduced in the materials.

### 5.7 Comparison between Theory and Experiment

5.7.1. Experiment

Co-Fe-Al-O nanogranular thin films with a thickness of approximately 0.1 μm were prepared by radio frequency magnetron sputtering in an $O_2$+Ar atmosphere to a background pressure better than $7\times10^{-7}$ Torr. The Ar/$O_2$ ratio was varied to change the oxygen content in the thin films. Co-Fe-Al composite targets composed of a Co-Fe alloy target and Al chips were used. The films were deposited on Si substrates in a static field of 1 kOe to induce uniaxial magnetic anisotropy. The film structure was investigated by x-ray diffraction using a Cu$K\alpha$ radiation and by high resolution transmission electron microscopy combined with energy dispersive x-ray spectroscopy. Magnetic properties were measured with a vibrating sample magnetometer. The FMR frequency was measured from the frequency dependence of the permeability up to 9 GHz. Magnetostriction was measured by the optical cantilever method under rotating in-plane fields up to 150 Oe. The electrical resistivity was measured using the conventional four-probe method.

5.7.2. Comparison with Theory

The theoretical permeability spectra are computed from Eqs. 59 and 60. In this computation, the values of the saturation magnetization, the anisotropy field, the electrical resistivity and the film thickness are taken from experimental results, and the damping constant is used as a fitting parameter. The complex permeability spectra of the films are measured when the exciting field is perpendicular to the easy axis. The thin films deposited under a magnetic static field exhibit a good uniaxial anisotropy.

The example of theoretical and experimental spectra of the complex permeability of as-deposited $(Co_{58}Fe_{35}Al_7)100_{1-x}$-$O_x$ film is shown in Fig. 24(a). A good agreement between theoretical and experimental results is observed. The real part of permeability is flat up to 1 GHz with a very low imaginary part of permeability and almost consistent with the calculations based on the experimental values of $4\pi M_S$, $H_K$, $\rho$ and $d$. The ferromagnetic resonance frequency is 2.3 GHz. The imaginary part is also in good agreement with the calculation. The deviation of $\mu''$ at around 2.3 GHz is noted. One reason may be that the calculation neglects the effect of local eddy currents, which occur due to impedance associated with capacitance between metallic particles separated by insulating interparticle regions. As another possible reason for this disagreement, it is the anisotropy dispersion caused by the irregularities in the domain structure, plus the effect of the complex but unknown morphology of the films.

Other measurements were done on a $(Co_{58}Fe_{35}Al_7)100_{1-x}$-$O_x$ film deposited under a static magnetic field. The hysteresis loops of this film measured under in-plane fields applied in the directions parallel and perpendicular to the induced anisotropy are shown in Fig 24(b). The film has a low $H_C$ in the easy and hard directions, and this small value of $H_C$ is attributed to the existence of some magnetic interaction among the granules which are well observed in the HRTEM image in Fig. 24(c). The crystalline (Co,Fe) grains (dark area) with a size of 3~5 nm are surrounded by a rather thick (several nm) amorphous Al-O matrix (gray area). The x-ray diffraction pattern of this film is shown in Fig. 24(d). The (110) diffraction peak from the bcc (Co,Fe) phase is seen, but no peaks are observed related with the oxides. This result indicates that Al-O is deposited as an amorphous phase, while Co-Fe is depos-

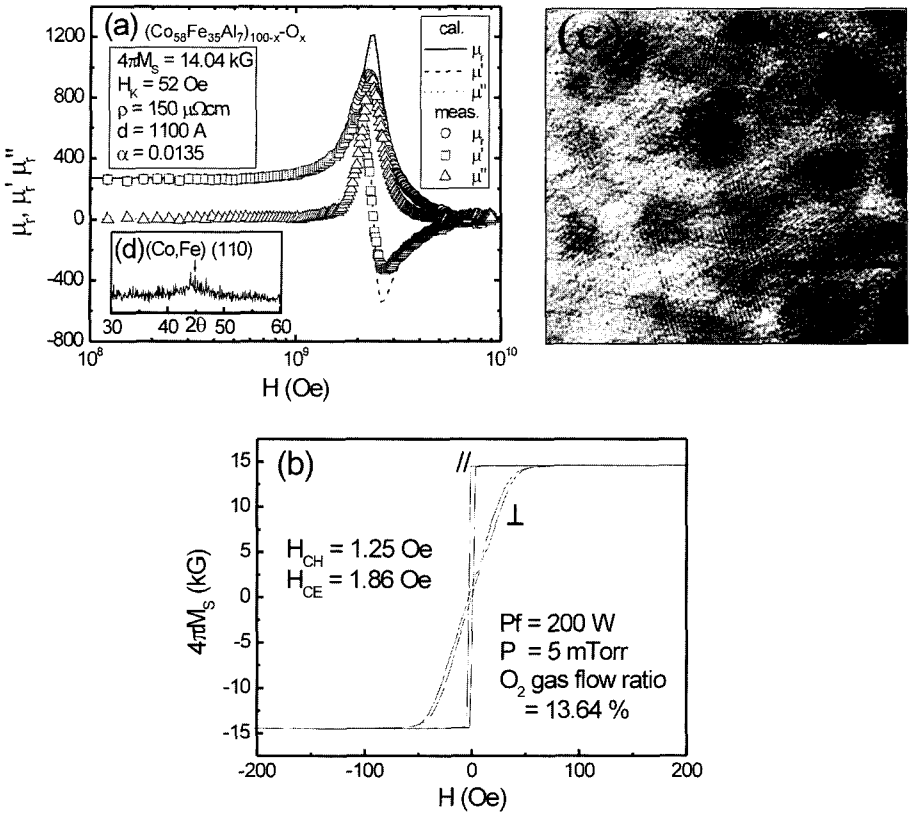


**Fig. 24.** (a) The frequency dependence of the permeability, (b) Hysteresis loops of the some experimental results for an as-deposited $(Co_{58}Fe_{35}Al_7)100_{1-x}$-$O_x$ film prepared at the RF power of 100 W, the working pressure of 5 mTorr and the $O_2$ flow ratio of 13.64 %; the hysteresis loops are measured under in-plane fields applied in the directions parallel and perpendicular to the induced anisotropy. (c) HRTEM image of as-deposited $(Co_{58}Fe_{35}Al_7)100_{1-x}$-$O_x$ film. (d) X-ray diffraction pattern of as-deposited $(Co_{58}Fe_{35}Al_7)100_{1-x}$-$O_x$ film.

ited without oxidation. The width of the (110) peak is large and the height is very small indicating a small grain size.

### 5.8 Artificially Controlled Shape Anisotropy

The main factor determining frequency characteristics of magnetic film is the ferromagnetic resonance frequency. As the ferromagnetic resonance frequency is proportional to the root of anisotropy field product the saturation magnetization (Eq. 21), the two values should be high;

$$f_R=\frac{\gamma}{2\pi}(H_K 4\pi M_S)^{1/2} \tag{21}$$

Moreover, a high electrical resistivity is also required to reduce the eddy current loss. Consequently, materials suitable for high-frequency application should have a large $M_S$ and $H_K$, which increase the ferromagnetic resonance frequency, and also a large $\rho$, which reduces eddy current loss. Among these three properties, only $H_K$ can be artificially controlled over a wide range by introducing shape anisotropy. A usual way to introduce artificially controlled shape anisotropy reported so far is a micropatterning of magnetic films [43-46].

If a ferromagnetic body of irregular shape is brought into a uniform applied field $H_0$, the actual magnetizing force $H$ inside the materials differs in magnitude from the applied field and varies in direction through the body. Inside any ellipsoid the component of $H$ along any principal axis $i$ is determined by the relation

$$H_i = (H_0)_i - N_i M_i,\ i = x,\ y,\ z \tag{61}$$

Where $M$ is the magnetization, and $N_i$ is a constant called the demagnetizing factor; it is determined by the ratios of the axes. Hence, if the magnetization components and the lengths of the axes of the ellipsoid are known, $H$ inside the body may be found. Calculation of $N$ for various axial ratios of the general ellipsoid will serve a useful purpose to introduce artificially controlled shape anisotropy to magnetic films. In Fig. 25, a very slender ellipsoid (c»b»a) employed in this study is shown. This shape

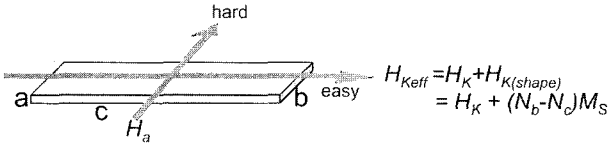


**Fig. 25.** A very slender ellipsoid considered in this study.

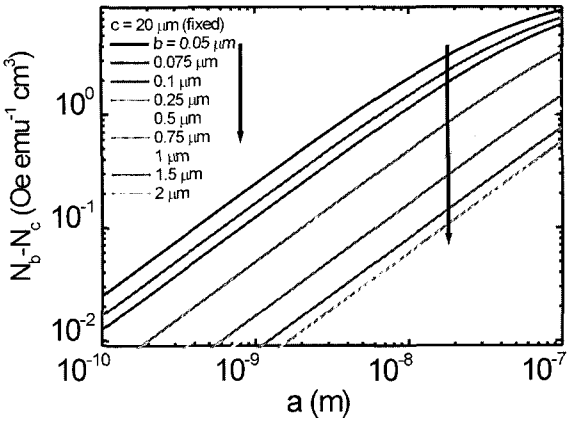


**Fig. 26.** Calculated values of $N_b$-$N_c$ as a function of the film thickness ($a$ axis) with the fixed $c$ axis of 20 μm and the variable $b$ from 0.05 μm to 2 μm.

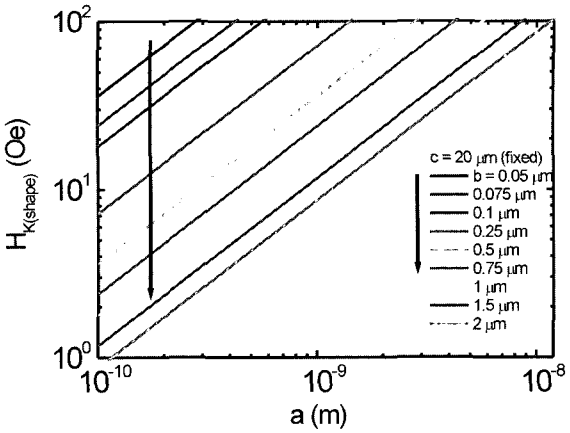


**Fig. 27.** Calculated values of shape anisotropy field as a function of the film thickness with $M_S$ of 1433 emu/cm$^3$ ($4\pi M_S$ = 18 kG), the fixed $c$ axis of 20 μm and the variable $b$ from 0.05 μm to 2 μm.

of the film is to increase the effective intensity of anisotropy field based on the increase of shape anisotropy energy. Practically, the width $b$, the length $c$ and the thickness $a$ of the film artificially control the shape anisotropy field. Then, the effective anisotropy field is equal to $H_{K(intrinsic)} + H_{K(shape)}$. $N_a$, $N_b$ and $N_c$ in Eq. 62 are the demagnetizing factors for magnetization along the three axes $a$, $b$, and $c$ of the slender ellipsoid;

$$N_a=4\pi\left[\frac{b}{a+b}-\frac{1}{2}\left(\frac{ab}{c^2}\right)\ln\left(\frac{4c}{a+b}\right)+\frac{ab(3a+b)}{4c^2(a+b)}\right]$$

$$N_b=4\pi\left[\frac{a}{a+b}-\frac{1}{2}\left(\frac{ab}{c^2}\right)\ln\left(\frac{4c}{a+b}\right)+\frac{ab(3a+b)}{4c^2(a+b)}\right]$$

$$N_c=4\pi\frac{ab}{c^2}\left[\ln\left(\frac{4c}{a+b}\right)-1\right] \qquad (62)$$

Thus the shape anisotropy field can be obtained as follows;

$$H_{K(shape)}=(N_b-N_c)M_S$$

$$=4\pi\left\{\frac{5a^2b+7ab^2+4ac^2}{4c^2(a+b)}-\frac{3}{2}\left(\frac{ab}{c^2}\right)\ln\left(\frac{4c}{a+b}\right)\right\}M_S \qquad (63)$$

Using Eqs. 62 and 63, the simulated $(N_b$-$N_c)$ and shape anisotropy field are shown as a function of the film thickness in Figs. 26 and 27, respectively. In Fig. 26, calculated values of $N_b$-$N_c$ are shown as a function of the film thickness with a fixed $c$ axis of 20 μm and the variable $b$ is varied from 0.05 μm to 2 μm. In that figure, one can know that the values of $(N_b$-$N_c)$ converge into $4\pi$ at a very high film thickness. As a film width increases, the values of $(N_b$-$N_c)$. In Fig. 27 calculated values of shape anisotropy field are plotted as a function of the film thickness with a $M_S$ of 1433 emu/cm$^3$ ($4\pi M_S$ = 18 kG), a fixed $c$ of 20 μm and the variable $b$ ranges from 0.05 μm to 2 μm. The curves in the figure have the same trends as

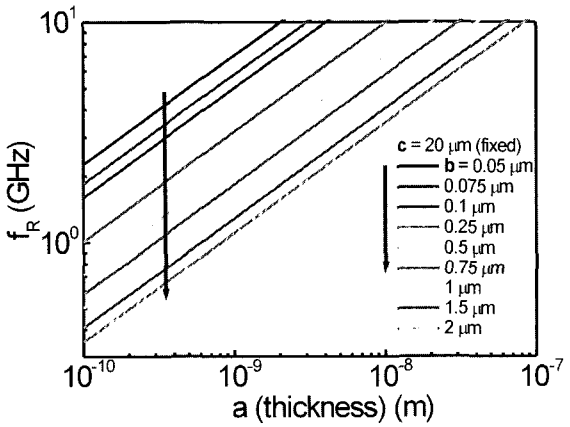


**Fig. 28.** Calculated values of ferromagnetic resonance frequency as a function of the film thickness with $M_S$ of 1433 emu/cm$^3$ ($4\pi M_S$ = 18 kG), gyromagnetic ratio $\gamma$ of 1.759 × 1011 T$^{-1}$s$^{-1}$, the fixed $c$ axis of 20 μm and the variable $b$ axis from 0.05 μm to 2 μm.

in Fig. 26. As the film thickness increases up to 0.1 μm, the shape anisotropy field increases monotonously without regard to the length of the film width. As the film thickness gradually increases, the free poles in the axis $b$, which is a metastable direction for spin to be aligned although most of free poles reside in the longest axis $c$, start to align in the axis $c$ since the axis b becomes no longer metastable. So, the shape anisotropy increases. When the film thickness becomes greater than the film width, most free poles residing in the width direction align in the length direction reaching the convergence of shape anisotropy field into the saturation value.

The ferromagnetic resonance frequency ($f_R$) and relative permeability ($\mu_r$) are simply obtained by substituting the results of Fig. 27 for $H_K$, assuming $H_{K(intrinsic)}$ = 0 Oe, into Eqs. 21 and 49, respectively.

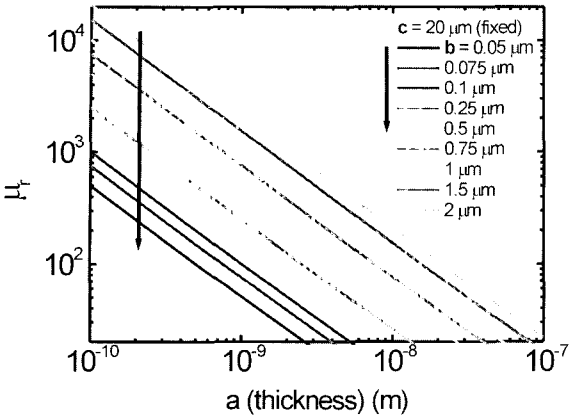


**Fig. 29.** Calculated values of relative permeability as a function of the 20 μm and the variable $b$ from 0.05 μm to 2 μm .

$$f_R=\frac{\gamma}{2\pi}\sqrt{H_K 4\pi M_S} \tag{21}$$

$$\mu_r=\frac{4\pi M_S}{H_K} \tag{49}$$

The values of ferromagnetic resonance frequency are calculated and shown in Fig. 28 as a function of the film thickness with a $M_S$ of 1433 emu/cm$^3$ ($4\pi M_S$ = 18 kG), a gyromagnetic ratio $\gamma$ of 1.759 × 1011 T$^{-1}$s$^{-1}$, a fixed $c$ of 20 μm. The variable $b$ ranges from 0.05 to 2 μm. As known in Eq. 21, the ferromagnetic resonance frequency is proportional to the anisotropy field and shows the same trends as those of the anisotropy field in Fig. 27. But the relative permeability is in inverse proportion to the anisotropy field as shown in Fig. 29. Both ferromagnetic resonance frequency and relative permeability have proportional relations with the saturation magnetization. Hence for obtaining high values of $f_R$ and $\mu_r$, thin films with a proper $H_K$ should be designed.

## VI. Concluding Remarks

This article has overviewed recent developments in high frequency magnetic thin films. The topic discussed is the magnetic and magnetostrictive properties of nanogranular Co-Fe-Al-O sputtered films: a particular emphasis on the high frequency applications.

The structure of nanogrnular (Co-Fe)-Al-O films is in the two-phase state and consists of a network of metallic grains (Co,Fe) rich in magnetic elements and non-metallic integrains (amorphous Al-O insulator) rich in light elements. The high resistivity arises from an electrical separation of the metallic grains by integrains. The nanocrystalline (Co-Fe)-Al-O films prepared by reactive sputtering in the static magnetic field to induce the uniaxial anisotropy exhibit about 18kG for $B_S$, about 60 Oe for $H_K$, over 300 μΩcm for $\rho$, about 0.5~1 Oe for $H_C$, over 250 for $\mu'$ up to around 1 GHz, and over 2 GHz for ferromagnetic resonance frequency, which are among the highest levels recorded among same for such thin films. The composition dependence of magnetostriction of granular films is similar to that of bulk Co-Fe alloys. The maximum magnetostriction (of the order of 40 ppm) along with a very good field sensitivity of magnetostriction is obtained in an equiatomic composition of Co and Fe. The magnitude of magnetostriction varies slightly with increasing annealing temperature up to 300°C. The results for the soft magnetic and magnetostrictive properties clearly indicate that the present thin film can be suitable for magnetoelastic applications in the high frequency range. One possible application under consideration is a surface acoustic wave device for wireless LAN (Local Area Network).

The complex permeability at high frequency of thin ferromagnetic films is considered when the magnetization is due to spin rotation. The frequency-dependence of the permeability of an uniaxial thin film with an in-plane anisotropy is calculated, using Eqs. 53 and 54. The parameters in these equations are the gyromagnetic factor, the damping constant, the anisotropy field, the saturation magnetization, the electrical resistivity, and the thickness of the magnetic films. The influence of intrinsic parameters such as magnetization, anisotropy field and damping constant on the permeability spectra is shown. And so is the influence of electrical resistivity and thickness of magnetic films. Increasing the value of $4\pi M_S$ increases the level of $\mu'$ at low frequency and $\mu''$ but does not change the roll-off frequency. Increasing the value of $H_K$ reduces the level of $\mu'$ and $\mu''$ and increases the value of the roll-off frequency. Reducing $\alpha$ increases the roll-off frequency. Increasing $\rho$ increases the level of $\mu'$ and roll-off frequency but does not change the level of $\mu'$ and roll-off frequency in very thin film with thickness of 0.1 μm. Decreasing the magnetic film thickness increase the roll-off frequency but does not change the level of $\mu'$ and $\mu''$ in low frequency ranges.

When the change in magnetization is fully determined by spin rotation, the agreement between the permeability calculated including eddy currents and FMR and the measured one is excellent. Ferromagnetic resonance is the most important loss mechanism for highly permeable films thinner than 1 μm.

Considering magnetization only due to domain rotation, the well-known expression for the resonance frequency, $f_R=\frac{\gamma}{2\pi}\sqrt{H_K M_S}$, can be derived from by substituting zero for $\mu$ in Eq. 47. And the relative permeability, $\mu_r=\frac{\mu_0 M_S}{H_K}$, can be derived from by substituting zero for $\omega$ in Eq. 47.

To increase the ferromagnetic resonance frequency, large $M_S$, $H_K$, and $\rho$ values are essential. But among these three properties, only $H_K$ can be artificially controlled over a wide range of its value by introducing shape anisotropy. The shape anisotropy field can be calculated by a simple equation.

$$H_{K(shape)}=(N_b-N_c)M_S \quad (63)$$

And the ferromagnetic resonance frequency ($f_R$) and relative permeability ($\mu_r$) are also simply obtained by substituting the results of Eq. 63 for $H_K$, assuming $H_{K(intrinsic)}$ = 0 Oe, in Eqs. 21 and 49, respectively. Hence for obtaining high values of $f_R$ and $\mu_r$, the shape of magnetic thin films with a suitable $H_K$ can be designed.

## References


[1] H. Okano, Y. Takahashi, T. Tanaka, K. Shibata and S. Nakano, Jpn. J. Appl. Phys., **31**, 3446 (1992).

[2] C. K. Campbell, *Surface Acoustic Wave Devices for Mobile and Wireless Communications* (Academic, New York, 1998).

[3] F. W. Voltmer, R.M. White, and C.W. Turner, Appl. Phys. Lett., **15**, 153 (1969).

[4] T. L. Tsai, S. D. Wu, G. Thomas, and H.S. Tuan, J. Appl. Phys., **48**, 4687 (1977).

[5] W. P. Robbins and J. Bowers, J. Appl. Phys., **50**, 78 (1979).

[6] W. P. Robbins, IEEE Trans. Sonics Ultrason. **SU-26**, 230 (1979).

[7] A. N. Aleseev and V. A. Ermolov, Sov. Phys. Acoust., **32**, 318 (1987).

[8] D. C. Webb, D. W. Forester, A. K. Ganguly, and C. Vittoria, IEEE Trans. Magn, **15**, 1410 (1979).

[9] S. Chikazumi, *Physic of Ferromagnetism* (Clarendon, Oxford, 1997), p. 371.

[10] H. Tomita, T. Inoue, and T. Mizoguchi, IEEE Trans. Magn. **32**, 4529 (1996).

[11] E. Quandt and A. Ludwig, J. Appl. Phys. **85**, 6232 (1999).

[12] S. H. Lim, Y. S. Choi, S. H. Han, H. J. Kim, T. Shima and H. Fujimori, IEEE Trans. Magn, **33**(5), 3940 (1997).

[13] Y. Shibata, Y. Kanho, K. Kaya, M. Kanai and T. Kawai, Jpn. J. Appl. Phys., **34**, L320 (1995).

[14] A. Hosono and Y. Shimada, J. Magn. Soc. Jpn., **12**, 295 (1988).

[15] M. Fujimoto, J. Am. Ceram. Soc., **77**, 2873 (1994).

[16] M. Fujimoto, Jpn. J. Appl. Phys., **32**, 5532 (1993).

[17] M. Fujimoto, T. Suzuki, Y. Nishi, K. Arai and S. Sekiguchi, J. Am. Ceram. Soc., **81**, 2477 (1998).

[18] V. Korenivski, J. Magn. Magn. Mater, **215-216**, 800-806 (2000).

[19] M. Yamaguchi, K. Suezawa, K. I. Arai, Y. Takahasi, S. Kikuchi, Y. Shimada, W.D. Li, S. Tanabe, and K. Ito, J. Appl. Phys., **85**, 791 (1999).

[20] J. Y. Park, S. R. Kim, J. Kim, K. Y. Kim, S. H. Han and H. J. Kim, J. Magn. Soc. Jpn., **23**(1-2), 243 (1999).

[21] H. J. Lee, S. Mitani, T. Shima, S. Nagata, and H. Fujimori, J. Magn. Soc. Jpn., **23**(1-2), 246 (1998).

[22] Y. Yosizawa, S. Oguma and K. Yamaguchi, J. Appl. Phys., **64**(10), 6044 (1988).

[23] S. Ohnuma, H. Fujimori, S. Mitani and T. Masumoto, J. Appl. Phys., **79**(8), 5130 (1996).

[24] S. Ohnuma, N.Kobayashi, T. Masumoto, S. Mitani and H. Fujimori, J. Magn. Soc. Jpn., 23(1-2), 240 (1999).

[25] S. Ohnuma, N. Kobayashi, T. Masumoto, S. Mitani and H. Fujimori, J. Appl. Phys., **85**(8), 4574 (1999).

[26] G. V. Skrotskii, L.V. Kubatov and S.V. Vonsovskii, *Ferromagnetic Resona*nce, Pergamon Press, F. Leccabue (1966).

[27] V. Siruguri, S. N. Kaul, J. Phys. Condens. Matter., **8**, 4567 (1996).

[28] R. Hasega, AIP Conf. Proc. **29**, 216 (1975).

[29] H. Puszkarski, Prog. Surf. Sci., **9**, 191 (1979).

[30] E. A. Turv, in S. V. Vonsovskii, *Ferromagnetic Resonance*, Pergamon Press, F. Leccabue, Oxford (1966).

[31] J. F. Cochran, K. Myrtle and B. Heinrich, J. Appl. Phys., **53**, 2261 (1982).

[32] V. Kanberky, B. Heinrich and D. Fraitova, Phys. Lett., **23**, 26 (1966).

[33] V. Kanberky and C.E. Patton, Phys. Rev. Bll, 2668 (1975).

[34] B. Heinrich, J.F. Cochran and R. Hasegawa, J. Appl. Phys., **57**, 3690 (1985).

[35] V. Kanbersky, Can. J. Phys., **48**, 2906 (1970).

[36] B. D. Cullity, *Introduction to Magnetic Materials* (Addison-Wesley, Reading, Massachusetts, 1972)

[37] W.S. Amento and G.T. Rado, Phys. Rev. **97**, 1558 (1953).

[38] D. Spenato, A. Fessant, J. Gierltowski, J. Loaec and H. LeGall, J. Phys. **D26**, 1756 (1993).

[39] E. Van de Riot and F. Roozeboom, J. Appl. Phys, **81**(1), (1997).

[40] L. Landau and E. Lifshitz, Phys. Z. Sowjetunion, **9**, 153 (1935).

[41] S. Chikajumi, *Physics of Magnetism* (Kinger, Boca Raton, Florida).

[42] E.C. Stoner and E.P. Wolfarth, Phil. Trans. R. Soc. A, 240 599 (1948).

[43] K.A. Ellis *et al.*, J. Appl. Phys, **87**(9), 6304 (2000).

[44] M. Munakata *et al.*, IEEE Trans., IEEE Trans. **3**(4), 2258 (2001).

[45] M. Yamaguchi *et al.*, IEEE Trans., **38**(5), 3183 (2002).

[46] M. Yamaguchi *et al.*, JMMM **215**, 807 (2000).

[47] N. Koayashi and S. Ohnuma, T. Masumoto, and H. Fujumori and J. S Pederson, J. Appl. Phys. **87**, 817 (2000).

[48] K. Ikeda, K. Kobayashi and M. Fujimoto, J. Am. Ceram. Soc., **85**(1), 160 (2002).

[49] M. Ohnuma, K. Hono, E. Onodera, S. Ohnuma, H. Fujimori and J. S. Pederson, J. Appl. Phys., **87**, 817 (2000).

[50] H. Hoffmann, J. Appl. Phys. 67,6981 (1990); G. Herzer, IEEE Trans. Magn. **MAG-25**, 3327 (1989).

[51] S. Ohnuma, N. Kobayashi, T. Masumoto and H. Fujimori, J. Magn. Soc. Jpn. Soc. Jpn, **22**, 441 (1998)

[52] A. Hosono and Y. Shimada, J. Appl. Phys., **67**, 6981 (1990); S. Ohnuma, H.J.N. Lee, N. Kobayashi, T. Masumoto and H. Fujimori; J. Magn. Soc. Jpn., **24**, 691 (2000).

[53] H. Karamon, T. Maumoto and Y. Makino, J. Appl. Phys., 57, 3527 (1985); H. Matsuyama, H. Egnchi and H. Karamon, J. Appl. Phys., **69**, 5123 (1990).

[54] E. Sugawara, F. Matsumoto, H. Fujimori and T. Masumoto, J.

Magn. Soc. Jpn, **16**, 247 (1992).
[55] A. Makino and Y. Hayakawa, J. Jpn. Inst. Met., **57**, 1301 (1993).
[56] R. M. Bozorth, *Ferromagnetism* (Van Nostrand, New Jersy, 1951).
[57] H.Warlimont and H.R. Hilzinga, in *rapidly Quenched Metals*, edited by T. Masamoto and K. Suzuki (Japan Institute of metals, Sendai, 1982). p. 1167.
[58] K. Nakanishi, O.Shimizu, and S. Yoshida, IEEE Trans. J. Magn. Jpn. **8**, 340 (1993).
[59] A. Hosono and S.tanabe, IEEE Trans. J. Magn. Jpn. **8**, 475 (1993).
[60] G. Y. Chin and J.H. Wernick, in *Ferromagnetic Materials*, edited by E.P. Wohlfarth, North-Holland, New York.